Physiol Rev
84: 385–410, 2004; 10.1152/physrev.00026.2003.

Pleural Mechanics and Fluid Exchange

STEPHEN J. LAI-FOOK

Center for Biomedical Engineering, University of Kentucky, Lexington, Kentucky

Lai-Fook, Stephen J. Pleural Mechanics and Fluid Exchange. *Physiol Rev* 84: 385–410, 2004; 10.1152/physrev.00026.2003.—The pleural space separating the lung and chest wall of mammals contains a small amount of liquid that lubricates the pleural surfaces during breathing. Recent studies have pointed to a conceptual understanding of the pleural space that is different from the one advocated some 30 years ago in this journal (Agostoni E. *Physiol Rev* 52: 57–128, 1972). The fundamental concept is that pleural surface pressure, the result of the opposing recoils of the lung and chest wall, is the major determinant of the pressure in the pleural liquid. Pleural liquid is not in hydrostatic equilibrium because the vertical gradient in pleural liquid pressure, determined by the vertical gradient in pleural surface pressure, does not equal the hydrostatic gradient. As a result, a viscous flow of pleural liquid occurs in the pleural space. Ventilatory and cardiogenic motions serve to redistribute pleural liquid and minimize contact between the pleural surfaces. Pleural liquid is a microvascular filtrate from parietal pleural capillaries in the chest wall. Homeostasis in pleural liquid volume is achieved by an adjustment of the pleural liquid thickness to the filtration rate that is matched by an outflow via lymphatic stomata.

I. INTRODUCTION

Since the last review that appeared in this journal some 30 years ago (1), the understanding of the fundamental concepts of the mechanics of the pleural space has undergone a continual evolution. The previous review invoked hydrostatic equilibrium of pleural liquid as the fundamental principle. In the current review, surface

forces due to the opposing elastic recoils of lung and chest wall are the primary determinants of the pressure in the intervening pleural liquid. The pleural surface pressure, defined as the force per unit pleural surface area, is equal to the pressure in the pleural liquid. The difference between the vertical gradient in pleural pressure and the hydrostatic value (1 cmH_2O/cm height) drives a viscous flow within the pleural space. A function of the liquid in the pleural space is to lubricate the pleural surfaces. The uniform thickness of the lubricating layer is maintained by recirculation of pleural liquid driven by gravity and ventilatory and cardiogenic motions. Pleural liquid is a microvascular filtrate that is cleared by pleural lymphatics, a process similar to that in the interstitium of all body organs.

The review is divided into the following sequence. A brief summary of regional volume and pleural pressure is presented, followed by a description of the different types of pleural pressure measurements. Then pleural liquid thickness is described within the context of pleural lubrication. Circulation of pleural liquid within the pleural space is treated as part of viscous flow theory. The next section describes the formation of pleural liquid as a microvascular filtrate and its absorption via lymphatic stomata. Finally, pleural liquid protein and the factors that determine its concentration and absorption are discussed.

A. Historical Perspective: Hydrostatic Equilibrium Versus Viscous Flow

The transmission of forces between the chest wall and the lung across the pleural space has been explained in two different ways. In the first, Setnikar et al. (180) and Agostoni et al. (14) proposed that pleural liquid, like the capillary blood, was in hydrostatic equilibrium with a vertical pressure gradient equal to 1 cmH_2O/cm height. They proposed that hydrostatic equilibrium was achieved by absorption of pleural liquid into the blood until a balance of hydrostatic and osmotic forces between pleural liquid and the blood occurred. The absorptive pressure was calculated to be -11 cmH_2O, lower than the surface pressure required to maintain the lung at its end-expiratory volume. The difference between pleural liquid and surface pressures was attributed to points of contact between the two pleural surfaces. This concept of the mechanics of the pleural space has been the focus of several reviews by Agostoni and co-workers (1, 2, 9, 18).

The second concept (97, 98, 103) is the one that I emphasize in this review. The surface pressure acting to expand the lung, equal and opposite to the pressure expanding the chest wall, is transmitted hydraulically across the thin pleural liquid space with the surface pressure equal to the pleural liquid pressure. Thus pleural surface pressure is the major determinant of the pleural liquid pressure. The difference between the vertical gradient in pleural surface pressure and the hydrostatic value drives a viscous flow of pleural liquid downward in the pleural space. This conception of the mechanics of the pleural space requires a continuous pleural liquid space with no pleural contact.

II. PLEURAL PRESSURE

A. Regional Lung Volume and Pleural Pressure

There is a consensus among investigators that regional lung volume within the intact thorax varies with body position relative to gravity. Early bronchospirometry studies in humans in the lateral decubitus posture demonstrated that the dependent lung has a smaller end-expiratory volume, a larger tidal volume, and larger regional ventilation than the nondependent lung (111). Studies by Milic-Emili and co-workers (90, 123) using external scintillation counting of inhaled radioactive xenon in humans confirmed that vertical gradients in regional lung volume and ventilation are also present in the upright and supine positions. Furthermore, in upright humans, the vertical gradient in transpulmonary pressure calculated from the vertical gradient in regional lung volume and the lung pressure-volume curve was found to be consistent with the vertical gradient of pleural pressure estimated by esophageal balloons (123). Differences in ventilation between the dependent and nondependent lung have also been demonstrated in recumbent humans during mechanical and spontaneous ventilation (169), during anesthesia and paralysis (171), and with diaphragmatic contraction (174). The radioactive xenon technique, applied effectively in humans, is not suitable for use in smaller animals because of its limited spatial resolution. A vertical gradient in regional alveolar size was measured in dogs frozen in the head-up (74) and supine (85) postures. Measurements of pleural surface pressure in experimental animals using a counter-pressure technique produced vertical gradients in transpulmonary pressure that were consistent with vertical gradients in regional lung volume (8, 12, 61–63). Comprehensive reviews of these studies have been written by Agostoni (1, 2).

Measurements of pleural pressure using a variety of techniques (see sect. II*C*) in experimental animals have demonstrated vertical gradients in pleural pressure in the head-up (35, 57, 83, 87, 89, 99, 189, 191, 214), head-down (57), supine (1, 2, 98, 159, 160, 175, 214–216), prone (175), and lateral decubitus (1, 2) positions. With few exceptions, the results of these studies were generally consistent with regional pleural surface pressure inferred from studies of the vertical distribution in regional volume. However, the measured vertical gradients in pleural pressure were often greater than the vertical gradient for a

fluid with the density of the lung (103). A structural (finite element) analysis by West and Matthew (210) of the effects of gravity on the lung modeled as a compliant solid showed a vertical gradient in transpulmonary pressure of 0.2 cmH_2O/cm height, close to the value for a fluid having the density of the lung. Thus vertical gradients in transpulmonary pressure greater than the one predicted from the lung density implied the contribution of forces in addition to lung weight. This was supported by studies in experimental animals that showed a reduced vertical gradient in pleural surface pressure on removal of the abdominal contents (1, 2).

The development of sophisticated imaging techniques with high spatial resolution provided evidence of regional differences in lung volume that were not detected by the previous techniques. Roentgenographic imaging of intraparenchymal lung markers in supine dogs showed vertical and cranial-caudal gradients of regional lung volume (88). Computerized tomographic imaging of regional lung density in the dog (82, 84), sloth (84), and human (32) demonstrated vertical gradients of regional lung volume in the supine position. These observations were generally consistent with previous measurements of pleural surface pressure. The imaging techniques also showed that lung volume was more uniform in the prone than in the supine position (Fig. 1), a behavior that was not detected in previous studies. The prone position was also found to have a more uniform blood flow distribution (25, 66, 211).

Following the structural studies of the effects of gravity on the lung (210), more complex models were developed to show the effects of the weight of the heart and abdomen on the vertical gradient in transpulmonary pressure in different body positions. In addition to the weight of the abdomen (1, 2), the effects of gravity on the heart have been shown to contribute to the vertical gradient in transpulmonary pressure, more in the supine and upright positions than in the prone and head-down positions. In the supine position, compression of the dorsal lung regions by the weight of the heart produced a relatively large vertical gradient in transpulmonary pressure (112). This effect was absent in the prone position, where the weight of the heart was supported by the sternum and had little effect on regional lung volume (24). A structural analysis that included the abdomen with a compliant diaphragm, in addition to the lung and heart, showed a caudal extension of the ventral region of the lung in the supine position that was absent in the prone position. This cranial-caudal extension of the ventral regions together with a cranial-caudal shortening of the dorsal regions due to the weight of the heart and abdomen produced a change in shape of the diaphragm in the supine position from that present in the prone position (see Fig. 1, *insets*), with only a relatively small effect on end-expiratory lung volume (73, 112).

In the upright position, compression of the caudal lung regions by the weight of the heart contributes to the vertical gradient in transpulmonary pressure. This effect of the weight of the heart was predicted using a structural analysis of the lung and heart (36). This prediction was verified experimentally by esophageal pressure measurements in the head-up dog in which the weight of the heart was increased by filling it with mercury (89). In the upright position, inclusion of the abdomen with a compliant diaphragm in the structural analysis showed a cranial-caudal lung extension by abdominal weight that increased the vertical gradient in transpulmonary pressure and the end-expiratory lung volume (73). The structural analysis also showed a smaller vertical gradient in the head-down than upright position. In the head-down position, the weight of the heart and abdomen compressed the entire lung and reduced the end-expiratory volume to near the residual volume, which resulted in a relatively small vertical gradient in transpulmonary pressure. This explana-

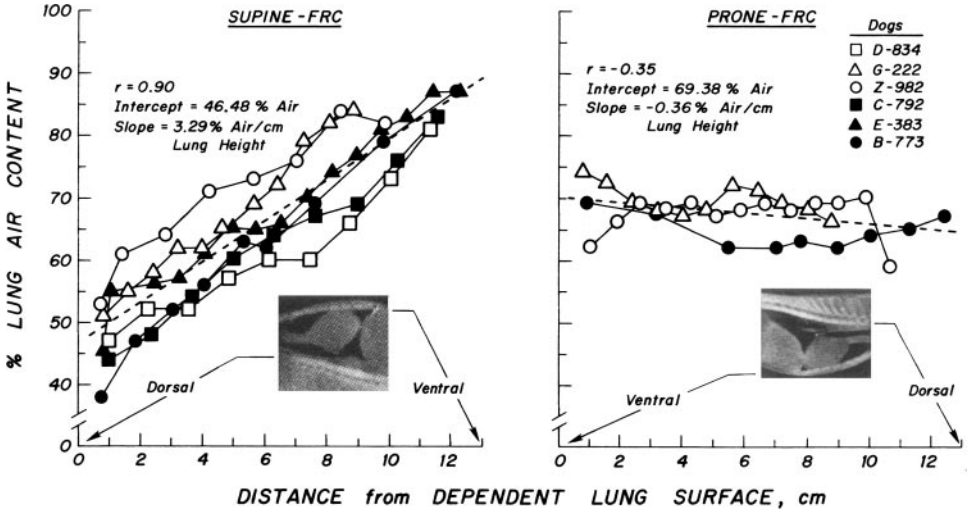

FIG. 1. Variation of lung air content with height measured in the anesthetized dog in the supine and prone position at functional residual capacity (FRC). Note the large variation of lung air content with height in the supine position compared with the constant value in the prone position. *Insets* show the change in shape in diaphragm surface from supine to prone positions. [From Hoffman (82).]

tion for the relatively small vertical gradient in the head-down position contrasts to that for the prone position, where support of the weight of the heart and abdomen by the sternum and spine, respectively, results in little change in regional lung volume.

Measurements of pleural liquid pressure using rib capsules implanted in dogs showed a greater vertical gradient in the supine than prone position (99, 214) and matched the behavior in pleural surface pressure inferred from measurements of regional lung volume (88) and density (82, 84). A similar behavior in pleural liquid pressure was measured in the pony (159) and rabbit (215, 216). However, these results in rabbits were supported by estimates of pleural surface pressure inferred from alveolar size (215, 216) but not by measurements of regional lung density (158, 160). Rib capsule measurements in the dog also showed a greater vertical gradient in pleural liquid pressure in the head-up than in the head-down position (99) that was similar to the behavior in pleural surface pressure predicted from the structural analysis (73). The noted exception notwithstanding, the agreement among the results of regional lung volume and density, structural analyses and rib capsule measurements of pleural liquid pressure supports the concept that pleural surface pressure is equal to pleural liquid pressure. Further support for this concept was provided by the rib capsule studies in which the pleural liquid pressure interpolated to midlung height was equal to the mean lung static recoil measured by the airway pressure after occluding the airway and opening the chest.

An unresolved issue is the effect of lung inflation on the vertical gradient in transpulmonary pressure. Some studies showed a reduced or constant vertical gradient in transpulmonary pressure (12, 87) with lung inflation, while other studies showed an increased gradient with lung inflation (36, 89, 216). In evaluating the effects of lung inflation, it is important to distinguish between the vertical gradient in regional volume and the vertical gradient in transpulmonary pressure. The vertical gradient in regional lung volume disappears with lung inflation because lung compliance becomes progressively smaller at higher transpulmonary pressures even in the presence of measurable vertical gradients in transpulmonary pressure.

More detailed reviews of regional lung volume and ventilation distribution have been published (122, 170). For the present purpose, the important conclusion is that regional lung volume distribution is determined by the interaction among the forces in the lung, thoracic and abdominal cavities attenuated by the effects of gravity that change with body position (170). In the supine and upright positions, there is a relatively large vertical gradient in regional lung volume that is produced by the combined effects of gravity acting on the lung, heart, and abdomen. In the prone position, the regional lung volume along the vertical axis is more uniform because the effects of gravity are relatively small. In the head-down position, vertical differences in regional volume are virtually absent in the highly compressed lung.

Pleural pressure couples the lung to the rib cage and diaphragm via a thin liquid film that lubricates the pleural surfaces during breathing. Because the vertical pleural pressure gradient is always less than the hydrostatic value, part of the gravity force drives a small viscous flow of liquid downward in the pleural space. This small flow does not affect the distribution of pleural surface pressure that is determined by the force balance between the lung and adjacent structures.

B. The Question of Pleural Contact

The controversy regarding force transmission across the pleural space was fueled by large differences between the vertical gradient of transpulmonary pressure and the vertical gradient of pleural liquid pressure measured by intrapleural catheters that was near the hydrostatic value. The first explanation of these differences was to postulate the existence of points of contact between the two pleural surfaces to make up the difference between pleural surface pressure and pleural liquid pressure (1, 2). In the absence of any experimental evidence of points of contact (7, 11, 13), contact through cells present in pleural liquid and microvilli was proposed (1, 2). Although some contact most likely occurs in the pleural space, the relevant question is whether its magnitude is sufficient to affect substantially the equality between liquid and surface pressures.

Perhaps the major objection to contact forces as an explanation for the differences between pleural surface pressure and pleural liquid pressure measured by intrapleural catheters is the prohibitively large pressures that have to be attributed to pleural contact. In small mammals of small lung height, such as the rat, contact pressures would be relatively small, of the same order of magnitude as pleural surface pressure (approximately -2 cmH_2O). However, in large mammals, such as humans, contact pressures would have to be much larger than pleural surface pressure. For example, consider an upright human with a vertical surface pressure gradient of 0.3 cmH_2O/cm (122) and a hydrostatic gradient in pleural liquid pressure (1 cmH_2O/cm). With the pressures at the lung base of 0 cmH_2O (6), the difference in pleural surface and liquid pressures at the lung apex located 30 cm above the lung base would be 21 cmH_2O, more than double the pleural surface pressure of 9 cmH_2O. It is unlikely that cells present in pleural liquid (127, 177) and microvilli (198–200) are numerous enough to account for this difference, since they occupy <1 and 3% of the surface area, respectively (see sect. III). Moreover, the required contact pressure would have to be even greater in animals larger than humans.

The concept of a hydrostatic gradient of pleural liquid pressure was accompanied by the need to postulate a net absorptive pressure for the pleural space to satisfy the Starling force balance for zero microvascular filtration required for hydrostatic equilibrium. As with contact points, there is little evidence for a net absorptive pressure in the pleural space (see sect. v). Accordingly, an alternative explanation based on viscous flow theory for the difference between the vertical gradient in pleural surface pressure and the hydrostatic value seems more plausible, particularly in view of evidence of flow redistribution occurring within the pleural space. Before the viscous flow theory is discussed as it applies to the mechanics of the pleural space, it is helpful to review various techniques for measuring pleural pressure because differences between pleural surface and liquid pressures might be attributed to the distortions introduced by the measuring devices themselves.

C. Measurements of Pleural Pressure

A definitive direct measure of pleural pressure has remained elusive because the pleural space is very thin, of the order of 5–35 μm (7, 11, 13, 27, 100, 101, 204, 202). This is demonstrated in Table 1, a summary of the vertical pleural pressure gradients measured in the head-up dog at end-expiratory lung volume by a variety of methods. Pleural liquid pressure was measured by the first three methods, and pleural surface pressure was measured by the remaining four methods. The vertical gradients range from 0.2 to 0.9 cmH_2O/cm height. The smaller values (0.2–0.3 cmH_2O/cm) were obtained with flat pleural balloons (87, 96, 118, 168), the larger values (0.7–0.9 cmH_2O/cm) with liquid-filled intrapleural catheters and needles (35, 57, 189). Intermediate values (0.4–0.5 cmH_2O/cm) for the pleural pressure gradient were measured by other methods: esophageal balloons (89, 191), counter pressure devices (1, 2), alveolar size measurements (74), and rib capsules (99, 214). The different methods will be discussed in turn with regard to their strengths and deficiencies.

The esophageal balloon is the only method that is suitable for measuring pleural pressure in humans (193). Indeed, it has been used extensively for measuring pulmonary airway resistance in clinical medicine and in experimental animals. Because the esophagus is oriented in a cranial-caudal direction in the mediastinal space between the lungs, the vertical gradient in pleural pressure can be measured by this method only in the upright and head-down body positions (89, 191). The limitation of this method is that the pressure measured is often attenuated by the stiffness of the esophagus due to smooth muscle tone and by the weight of the surrounding mediastinal structures. As a result, the pressure measured is a function of the balloon's location within the mediastinal space and of body position and often produces unreliable values for the lung static recoil (37).

TABLE 1. *Vertical gradient in pleural pressure measured in head-up dogs*

Method	Gradient, cmH_2O/cm	Reference Nos.
Pleural needle	0.93	189
Pleural catheter	0.72	35, 57
Rib capsules	0.53	99, 214
Alveolar size	0.50	74
Esophageal balloon	0.42	89, 191
Counter-pressure device	0.40	1, 2
Pleural balloon	0.20–0.30	87, 96, 118, 168

[Modified from Lai-Fook and Rodarte (103).]

Intrapleural liquid-filled catheters, rigid cannulas, and needles are relatively easy to implement and have been extensively used to measure pleural liquid pressure in experimental animals (1–3, 9, 7, 13, 20, 22, 23, 35, 57, 128, 129, 131, 139, 140, 175, 176). There are two reasons why intrapleural catheters produce vertical gradients in pressure near to the hydrostatic value (103). First, the liquid layer adjacent to a 1-mm-diameter intrapleural catheter is ~50-fold thicker than the normal pleural space and forms a static liquid column along the catheter. A similar effect occurs at the relatively wide spaces adjacent to lobar margins (91, 98; Fig. 5). In practice, vertical gradients measured by intrapleural catheters were often less than hydrostatic (35, 57, 139, 175, 176), although some investigators have consistently measured a hydrostatic gradient with this technique (1, 2, 7, 13). Second, an abnormally thick pleural space also would exist distal to the tip of the catheter. Thus a catheter situated near a lobar margin would be determined partly by the pressure at the lobar margin, where a hydrostatic gradient exists (Fig. 2). Intrapleural wick catheters have been used in an attempt to reduce the distortion of the pleural space, but like intrapleural catheters, they also spread apart the pleural space and often produced results similar to those measured by intrapleural catheters (83).

A number of techniques have been developed to circumvent the problems associated with intrapleural catheters. They each have advantages and disadvantages.

Flat air-filled pleural balloons (87, 117, 118) have been used to measure the average recoil of the lung region adjacent to the surface of the balloons. The placement of a flat balloon into the pleural space causes an indentation of the lung surface that reduces the recoil of the lung adjacent to the balloon and the vertical gradient in pleural pressure (78, 103, 214). Moreover, the chest must be opened to install pleural balloons, and any residual air in the pleural space that is not removed on closing the chest compresses nondependent lung regions. For the above reasons, the vertical gradients in pleural pressure mea-

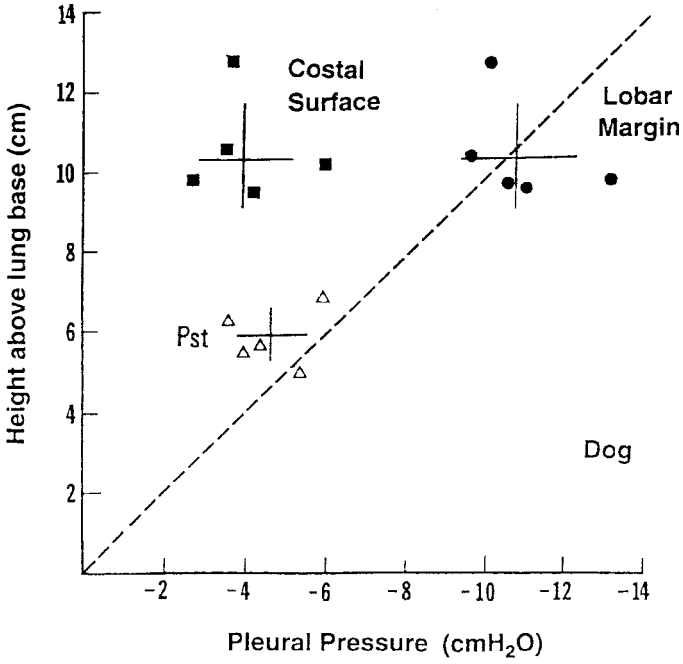

FIG. 2. Pleural liquid pressure measured in the prone dog at a lobar margin and costal surface in the nondependent thorax, and mean lung static recoil (Pst). Note that pressure at the lobar margin fell along the line of identity that represented the hydrostatic gradient, while pressure at the costal surface was less negative and equal to Pst. [Modified from Lai-Fook (97).]

sured by flat pleural balloons are relatively small (0.2–0.3 cmH_2O/cm).

In the counter-pressure method for measuring pleural surface pressure, a negative pressure is applied to a parietal pleural window located in the intercostal space until the lung surface becomes flat (1, 2, 8, 12). This method assumes that the undisturbed lung surface is usually flat, whereas the intercostal lung surface is normally depressed inwards due to the smaller intercostal muscle recoil compared with the ribs (86). Thus the magnitude of the counter pressure taken as the pleural surface pressure would differ from that required to produce a normally curved pleural surface.

Pleural pressure can be estimated by comparing regional alveolar volume measured in vivo to the pressure-volume behavior measured in the isolated lung (61, 215, 216). The measurement of alveolar size through parietal pleural windows also requires the removal of intercostal muscle, and therefore, the lung region beneath the window has reduced elastic recoil. In spite of these limitations, these techniques for measuring pleural pressure produced results that were in general consistent with measurements of lung volume distribution.

Two methods, the micropuncture (98, 129) and rib capsule techniques (99, 159, 160, 214, 216), have been used to measure pleural liquid pressure with minimal distortion of the pleural space. In the micropuncture technique, pleural liquid pressure is measured in conjunction with a servo-nulling device through a micropipette tip (2–5 μm diameter) that is smaller than the pleural space thickness. Like the techniques that measure a counter pressure and alveolar size, the micropuncture technique requires the removal of intercostal muscle to puncture the parietal pleura, which would reduce the local lung elastic recoil. Because the micropipette tip is difficult to visualize in tissue, its exact location cannot be determined with certainty. Furthermore, pleural pressure can be measured only during apnea because the glass micropipette is easily broken.

In the rib capsule technique, a capsule is implanted in a rib and a small hole is made in the parietal pleura to allow pressure communication between the liquid in the capsule and the pleural liquid. The rib capsule is similar in concept to the intercostal capsule (10), but the rib capsule technique avoids the reduced recoil caused by removal of intercostal muscle. A limitation of the rib capsule technique is that measurements are confined to the pleural space under ribs, where pleural pressure might be slightly less than that beneath intercostal muscle because of the stiffer rib (86).

D. Pleural Pressure at Lobar Margins and Zone of Apposition of Rib Cage to the Diaphragm

1. Lobar margins

Although a hydrostatic gradient in pleural pressure is not generally attained in the pleural space, there are spaces such as at lobar margins where a hydrostatic gradient is established (91, 98). A cross-section of a lobar margin in the rabbit measured using the light microscopic-focusing technique (101) is shown in Figure 5 (see sect. IV). Note that the pleural liquid thickness adjacent to the margin of the middle lobe is much greater than that on the flat costal surface. The reason for the hydrostatic gradient, within the context of viscous flow concepts (see sect. IV) is that at lobar margins the pleural space is wide enough so that the viscous losses are negligible, similar to the effect observed in blood capillaries. Also at lobar margins the vertical gradient in pleural liquid pressure is matched by the appropriate vertical variations in lung surface curvature and pleural membrane tension that are not possible on the relatively flat costal lung surface. Micropuncture measurements of pleural liquid pressure in the nondependent region of prone rabbits (98) and prone dogs (91) showed the pressure at the lobar margin to be more negative than on the costal surface (Fig. 2). Similar results were obtained using rib capsules (194).

Under conditions of apnea in nondependent regions, where pleural liquid pressure at the lobar margin is more negative than the pressure on the adjacent costal surface (Fig. 2), pleural liquid flows from the costal surface to the

lobar margin regions. The difference between the costal surface pressure and the lobar margin pressure decreases with distance down the lung. This should result in an increased pleural space thickness down the lung, a behavior not substantiated by the uniform pleural space thickness measured (7, 27, 101). However, the costal surface-to-lobar margin flow that occurs during apnea is offset by a ventilation-induced reverse flow (see sect. IV).

2. Zone of apposition of rib cage to the diaphragm

In the zone of apposition of the diaphragm to the rib cage, pleural pressure increases during spontaneous inspiration (3, 166, 194). This behavior resembles that of abdominal pressure (1, 2) and is opposite to that of pleural pressure on the lung surface, which decreases on inspiration. Thus the vertical gradient in pleural pressure in the zone of apposition is near the hydrostatic value and similar to the vertical gradient in abdominal pressure (3, 113).

III. PLEURAL LIQUID THICKNESS AND LUBRICATION

In terms of lubrication of the pleural surfaces, pleural liquid thickness is important to the evaluation of pleural contact and of the magnitude of shear stress induced during ventilation. Two types of pleural lubrication have been postulated. One is fluid lubrication based on viscous shear stresses developed in a fluid layer interposed between sliding surfaces (46). The second is boundary lubrication where the fluid layer thins so that part of the surfaces comes into contact.

A. Ventilation, Microvascular Filtration, and Energy Dissipation

For fluid lubrication in its simplest form, the forces that are generated by the sliding between the lung and chest wall during breathing are given by Newton's law of viscosity (46)

$$\sigma = \nu V/h \qquad (1)$$

The shear stress (σ) in pleural liquid is related to the lung-chest wall relative velocity (V), pleural liquid viscosity (ν), and pleural liquid thickness (h). The advantage of fluid lubrication is that resistance to motion arises from fluid viscosity, and friction on the pleural surfaces is virtually absent.

Pleural liquid thickness measured by a variety of techniques is extremely thin, varying between 5 and 35 μm. These techniques included light microscopic imaging of frozen samples (7, 11, 13), electron microscopy (27), light microscopic focusing (100, 101), and fluorescent imaging (204, 202). Generally pleural liquid thickness was uniform with respect to height in the thorax, except for a slight gradient in the sheep (27), and at lobar margins (27) and the lung base where it was much thicker (101). In our study (101), pleural liquid thickness during apnea increased with animal size, ranging from 7 μm in the mouse to 23 μm in the dog. The allometric relationship (182, 183) between pleural liquid thickness and animal mass (M) was (101): $h \propto M^{0.20}$ (Fig. 3).

1. Effect of ventilation

The imaging of fluorescent dye injected into the pleural liquid of rabbits showed that pleural liquid thickness increased with ventilation (204, 202). In this technique, the thickness of the pleural space was measured from the fluorescent light emitted by the pleural liquid through a parietal pleural window made in the intercostal space. Pleural liquid thickness measured from the fourth intercostal space was minimal (11 μm) during apnea and increased to ~35 μm with increases in tidal volume (202). A similar behavior was observed with increases in venti-

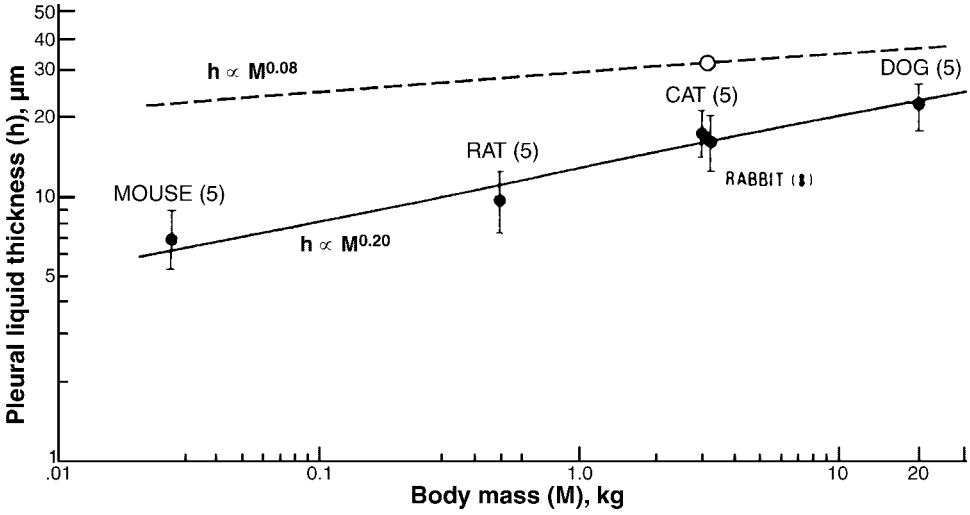

FIG. 3. Pleural liquid thickness (h) versus body mass (M) measured by light microscopy in five laboratory species during apnea. Note that thickness increased with body mass during apnea: $h \propto M^{0.20}$, consistent with pleural liquid filtration that scales with body mass (solid line). Dashed line is the allometric relation ($h \propto M^{0.08}$) predicted for ventilation with the assumption of a constant pleural liquid shear stress among species. Point (open circle) is the value measured in rabbits during mechanical ventilation. [Modified from Lai-Fook and Kaplowitz (101).]

lation frequency. This behavior was qualitatively consistent with a ventilatory pump (see sect. IV) that drives pleural liquid from the lobar margins to the flat costal surfaces, a behavior opposite to that expected during apnea (54). In subsequent studies, the thickness of the pleural space was measured using the fluorescent dye technique at three pleural windows located along the cranial-caudal axis (204). These studies showed that pleural liquid thickness increased along the cranial-caudal axis from a minimal value of 5 μm in the second intercostal space to a value of ~30 μm in the fifth intercostal space (Fig. 4*A*). This cranial-caudal gradient in pleural liquid thickness increased with ventilation, primarily due to an increased thickness in the caudal regions. The amplitude of lung velocity relative to that of the rib cage also showed a similar gradient that increased with frequency (Fig. 4*B*). This behavior is predictable from a uniform lung expansion caused predominantly by diaphragmatic contraction (119). Since the increase in pleural liquid thickness offset the increase in relative velocity (*Eq. 1*), shear stress amplitude in pleural liquid was constant with cranial-caudal distance but increased with ventilation frequency (Fig. 4*C*).

Three factors might contribute to the cranial-caudal gradient in pleural liquid thickness and constant shear stress. First, redistribution of pleural liquid associated with a ventilation-induced flow from lobar margins (see sect. IV) would be greater for the caudal lobe with a greater lung-chest wall relative velocity than for the cranial lobe. Second, a cranial-caudal gradient in pleural liquid thickness might be matched by a cranial-caudal gradient in filtration (see sect. V). Third, the lung within the chest wall might act like a shaft in a cylinder under load (46) where the load (P_o) caused by lung buoyancy (76) forces the lung against the chest wall. By fluid lubrication theory (46), the distance of nearest approach of the lung to the chest wall is proportional to $\nu V/P_o$ so that pleural liquid thickness increases with relative velocity (V) which increases with cranial-caudal distance.

A limitation of the microscopic focusing and fluorescent dye techniques is that a parietal pleural window is required. Accordingly, pleural liquid thickness measured through pleural windows might be affected by the reduced lung static recoil beneath the window (204). Given the small size of the window (2 mm diameter), the local recoil would depend more on the membrane tension and less on the intercostal muscle dissected (78). Furthermore, since any reduced recoil was constant, it is unlikely to account for the measured changes with frequency or cranial-caudal position.

Under apneic conditions pleural liquid thickness increased with animal size, $h \propto M^{0.20}$ (Fig. 3). This allometric relationship was explained by a pleural liquid filtration rate that scaled with body mass (101), with the assumptions of a constant net driving pressure gradient and a downward flow of pleural liquid that represents the filtration rate (see *Eq. 2*, sect. IV). A pleural liquid filtration rate of 0.01–0.02 $ml \cdot h^{-1} \cdot kg^{-1}$ (see Table 7) has been estimated in the sheep (212), dog (124, 152), and rabbit (48).

With the assumption that during ventilation shear stress in pleural liquid is constant among species, the allometric relationship is (104) $h \propto M^{0.08}$ (Fig. 3). Thus, during ventilation, the increase in pleural liquid thickness with body mass would be smaller than that measured during apnea.

Based on the pleural space thickness of the rabbit

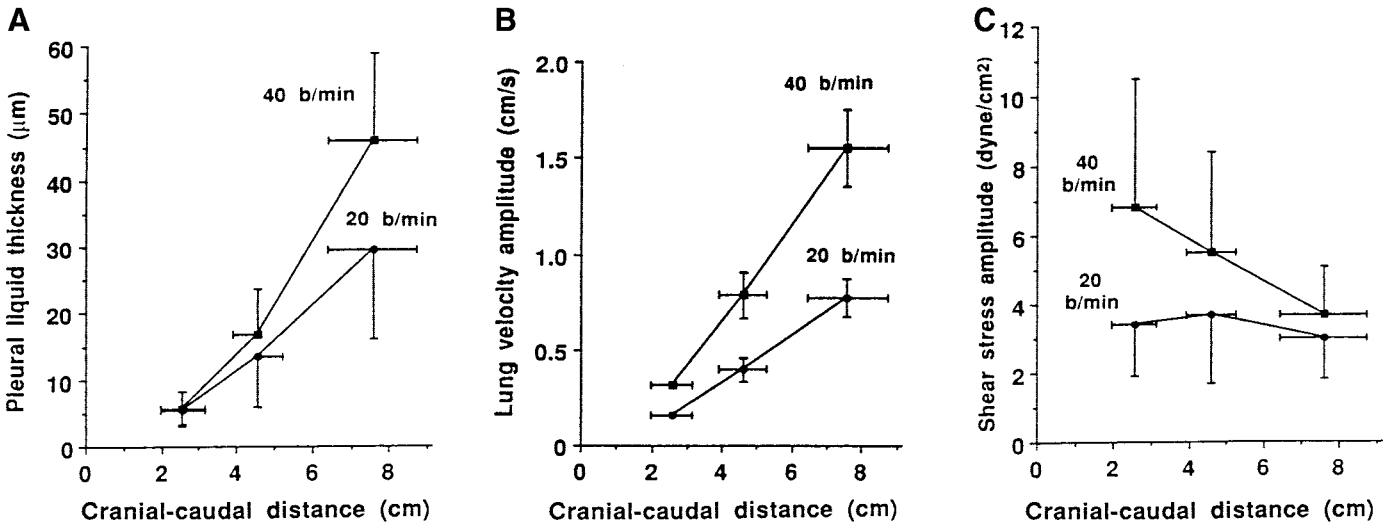

FIG. 4. Pleural liquid thickness (*A*), lung-chest wall relative velocity amplitude (*B*), and pleural liquid shear stress amplitude (*C*) versus cranial-caudal distance. Note that both thickness and velocity increased with cranial-caudal distance. This behavior produced a constant shear stress with cranial-caudal distance. [Modified from Wang and Lai-Fook (204).]

measured with mechanical ventilation (Fig. 4*B*), the two allometric curves converge as body mass increases (Fig. 3). This is because as breathing frequency is reduced with body mass (frequency $\propto M^{-0.25}$; Refs. 182, 183), conditions of apnea are approached. The intersection of the two curves occurs at an h value of ~60 μm and M of ~2,000 kg. This suggests that very large animals with a relatively low breathing frequency have a thickness during breathing equal to that of apneic conditions. The adult elephant and whale fall into this category. In one study (53), the pleural space of an adult elephant was found to be filled with interstitial-like tissue, in contrast to the fetal elephant with a normal pleural space (67). The need to breathe with the thorax submerged in water has been proposed as the reason for the liquid-to-tissue transformation of the elephant's pleural space (209). However, anecdotal accounts describe the whale's pleural space to be similar to most mammals, except for the cranial region where the pleural surfaces are fused (186).

2. Microvascular filtration

The relationship between pleural liquid thickness and filtration was examined in spontaneously hypertensive rats (100). Pleural liquid thickness measured in the hypertensive rats was 40% greater than the thickness measured in normotensive rats (10 μm). The increased thickness together with a reduced pleural liquid protein concentration was attributed to increased filtration caused by the higher vascular pressure in the hypertensive rats (45, 100).

3. Energy dissipation

The magnitude of the energy loss during breathing is crucial to any theory of force transmission across the pleural space. If only viscous losses due to sliding between uniformly spaced pleural surfaces were considered, a piston-in-cylinder model of the lung within the thorax would predict a power loss that is 1–2% of the work of breathing (101). Much higher energy losses (35%) have been estimated due to frictional forces of pleural contact (47). Fluid lubrication affords the more efficient mechanism for force transmission across the pleural surfaces during breathing.

B. Pleural Liquid Volume and Cell Composition

1. Pleural liquid volume

The volume of liquid collected from the pleural space in several adult species is listed in Table 2. Pleural liquid volume per unit body mass (V_{pl}) was found to decrease with body mass (M) according the allometric equation: $V_{pl} = 0.39M^{-0.63}$ ($n = 11$, $R^2 = 0.68$, $P < 0.001$).

TABLE 2. *Volume of pleural liquid*

Species	Body Weight, kg	Pleural Liquid Volume, ml/kg	Reference Nos.
Rat	0.45	0.6	137
Puppy	0.8	1.33	137
Cat	1.7	0.28	137
Rabbit	2.3	0.22	137
Rabbit	2.2	0.20	19, 127
Rabbit	3.3	0.13	48, 177
Rabbit	3.7	0.09	207
Dog	14	0.10	120
Dog	9	0.06	127
Dog	9	0.06	137
Pig	24	0.04	137
Sheep	32	0.13	49, 212

2. Cell composition

Similar to interstitial liquid of other organs (34), pleural liquid contains protein (mainly albumin, globulin, and fibrinogen) and a few cells (mainly mesothelial cells, monocytes, and lymphocytes) (127, 177). Albumin (~50%) comprises most of the protein followed by globulin (~35%). The cell concentration found in dogs and rabbits is ~2,000 cells/mm^3 volume of pleural liquid. These cells would occupy only ~1% of the pleural surface area. This value was based on a mean cell radius of ~10 μm (196, 199), a lung surface area of 300 μm^2 occupied by one cell, a pleural liquid volume in rabbits of 0.4 ml (Table 2), and lung surface area of 200 cm^2 (127). Thus cells present in pleural liquid would have a negligible effect on the force balance across the pleural space and could not account for the large contact stresses postulated.

C. Microvilli: Spatial Distribution

The pleural surfaces are lined by a layer of microvilli, 1–6 μm long depending on species and 0.1 μm thick (28, 29, 33, 115, 196). The physiological importance of microvilli in relation to pleural liquid filtration and pleural lubrication, and the role of microvilli in reducing pleural liquid shear stress, continue to be speculative. It is of interest that more microvilli are found in the caudal than in the cranial regions of the lung and chest wall surface (196), in parallel to the changes in lung-chest wall relative velocity during ventilation (Fig. 4*A*). Microvilli have been postulated to support contact forces between the pleural surfaces, and thus account for part of the difference between liquid and surface pressures (1, 2). Like the cells in pleural liquid, the number of microvilli (average of 300 per 100 μm^2, Ref. 33) seems too small to occupy a significant contact area (~3% of the total area).

D. Hyaluronan as a Pleural Lubricant

Hyaluronan has been identified as a coating on pleural mesothelial cells (70, 107) and has been proposed as a

boundary lubricant (1, 2). A similar function has been attributed to surfactant present in pleural liquid (80, 81). The turnover of hyaluronan in the rabbit pleural space is ~1 day (30). Pleural liquid hyaluronan does not contribute to fluid lubrication because its concentration in pleural liquid (0.7 μg/ml) is too small to change pleural liquid viscosity significantly from that of water (30). The amount of hyaluronan present in the pleural tissue measured by lavage in rabbits was 0.1 mg/kg body wt (207), considerably greater than that present in the pleural liquid. Hyaluronan in pleural liquid probably originates in the mesothelial cells and pleural tissue (207), although other sources, such as lung liquid, are possible (51, 52).

The effect of ventilation on hyaluronan present in pleural liquid was studied in anesthetized and conscious rabbits (205). In conscious rabbits placed in a box, the increase in hyaluronan concentration in pleural liquid measured over 24 h was faster with a hypercapnic-induced increase in ventilation than with room air ventilation. In the anesthetized rabbits, hyaluronan concentration in pleural liquid doubled with a twofold increase in ventilation. The increase in hyaluronan concentration was attributed to an increase in the production of hyaluronan from pleural tissue rather than to a washout effect of increased filtration, an effect that has been demonstrated in lung lymph studies (109). In studies of rabbits ventilated post mortem with no filtration, pleural tissue hyaluronan doubled in conjunction with a 30% reduction of pleural liquid volume (207). The increased hyaluronan was attributed to the increase in pleural liquid shear stress imposed on the mesothelial cells with a reduced pleural liquid thickness. Because hyaluronan recovered by lavage was ~1,000-fold greater than that present in the normal pleural liquid, most of the increased hyaluronan was probably sequestered within the tissue or trapped on the mesothelial cell surface and between microvilli.

The role of hyaluronan in pleural lubrication remains speculative. One proposal is that glycoprotein rich in hyaluronan and enmeshed in microvilli (33) acts like a boundary lubricant in the event of depletion of pleural liquid. The unique properties of hyaluronan-rich solutions (156) that resist motion at low shear rates but lower viscosity and shear stress at high shear rates might be crucial during breathing (1, 2). However, the shear modulus (~1 cmH_2O) of hyaluronan solutions (156) seems too small to support the large contact stresses that have been postulated.

IV. CIRCULATION OF PLEURAL LIQUID

In the absence of pleural contact, gravity drives a flow of pleural liquid downward in the pleural space. Since all studies show a uniform pleural space thickness, there must be a continuous redistribution of pleural liquid from dependent to nondependent regions. A model of pleural liquid recirculation has been proposed (54) with the following elements: a gravity-dependent downward flow of pleural liquid on the flat costal surfaces, an upward flow along lobar margins, and a transverse flow from lobar margins to the flat costal surfaces.

A. Gravity-Dependent Flows: Absence of Hydrostatic Equilibrium

The forces driving flow downwards in the pleural space result from the vertical gradient in surface pressure distribution determined by the opposing recoils of the lung and chest wall and the force of gravity acting on the pleural liquid. Consider steady unidirectional viscous flow of liquid between the two pleural surfaces modeled as two vertical parallel plates separated by thickness h. The following equation relating pressure (P) in the liquid to flow (Q) downwards in the direction of gravity is known from fluid mechanics (97, 98, 103)

$$\rho g - dP/dz = 12\nu Q/(Lh^3) \quad (2)$$

where dP/dz is the gradient in pressure in the downward z-direction, ρg is the gravitational force per unit height acting on the liquid, and L is the lateral dimension. The left-hand side of *Equation 2* represents the net force driving flow downward. It is balanced by the term on the right-hand side of *Equation 2*, the viscous pressure losses due to flow per unit height. When the viscous losses are negligibly small, *Equation 2* reduces to $dP/dz = \rho g$, Pascal's law for a liquid at rest.

Consider the plates to be the lung and chest wall with the opposing elastic recoils that produce a pleural surface pressure gradient dP/dz. Because the compliance of the lung and chest wall is relatively large and the pleural space volume is extremely small, changes in pleural space thickness have a negligible effect on the pleural surface pressure. Thus the net pressure gradient, $\rho g - dP/dz$, is unaffected by the flow or thickness. A change in flow must therefore be accompanied by a change in thickness to maintain the viscous pressure losses constant. For example, in the prone position, where the pleural pressure gradient (dP/dz) is zero, the viscous flow and pleural space thickness adjust so that the viscous pressure losses exactly balance the gravitational force on the liquid. These conditions were simulated in a model of the pleural space consisting of a cylindrical-shaped balloon expanded within a rigid cylinder (102). Pleural pressure of the model, equal to the balloon recoil, was uniform along the height of the balloon, where the balloon was expanded to a uniform diameter and the pleural space was extremely thin, but varied by 1 cmH_2O/cm height at the two ends of the balloon, where the space was relatively

wide and the balloon recoil was nonuniform. If the pleural pressure gradient (dP/dz) were to equal 0.6 cmH_2O/cm, as measured in the supine position of many species (1, 2), the net driving pressure would be 1 − 0.6 = 0.4 cmH_2O/cm and the viscous losses would be 0.4 cmH_2O/cm.

For a constant driving pressure, the flow (Q) depends directly on h^3. If h is halved, Q is reduced eightfold. Thus the flow vanishes as the space thins to small values. In *Equation 2*, the channel is assumed to be uniform in thickness. However, as applied to the real pleural space, nonuniformities in thickness may significantly increase the flow resistance. For example, in the balloon-in-cylinder model of the pleural space (102), the measured flow was two orders of magnitude less than that predicted for a uniform channel. Thus nonuniformities in thickness resulting in a vanishingly small pleural liquid flow might explain in part why under apneic conditions the measured pleural liquid thickness appeared to reach a minimum value and was uniform with respect to height (102). The presence of microvilli and cells in the pleural liquid would also serve to increase flow resistance in the pleural space (1, 2).

Other models of viscous flow within the pleural space include the buoyancy forces exerted on a rigid chest wall by a rigid lung of density lower than the pleural liquid (76, 77). This model predicts a vertical gradient in pleural liquid thickness that is not supported by the uniform thickness with height measured (7, 27, 101). The model of the pleural space as a porous material (142) does not match the physical characteristics of the pleural space, except perhaps in the case of the adult elephant, whose pleural space reportedly becomes filled with an interstitial-like tissue (53).

B. Upward Flow Along Lobar Margins

Redistribution of pleural liquid from the lung base to the upper regions of the pleural space occurs through the widened pleural space formed at lobar margins. The pleural liquid thickness profile measured by light microscopic focusing (97) is shown in Figure 5, *inset*. Note that the pleural space is considerably wider immediately adjacent to the lobar margin, ~100 μm, and falls off monotonically with distance from the margin to a value of 15 μm at the costal surface. At lobar margins, the increased pleural space ensures that viscous forces are negligible, resistance to flow is small, and the vertical gradient in pleural pressure approaches the hydrostatic value. The small flow resistance is the reason why the distribution of an injected bolus into the pleural space occurs primarily via lobar margins (140). Studies in rabbits using fluorescent microbeads (6 μm diameter) to visualize flow demonstrated that cardiogenic and ventilatory motions act like a pump to move pleural liquid upwards at lobar margins while downward motion occurs on the costal surface distant from the lobar margin (Fig. 5, Ref. 201).

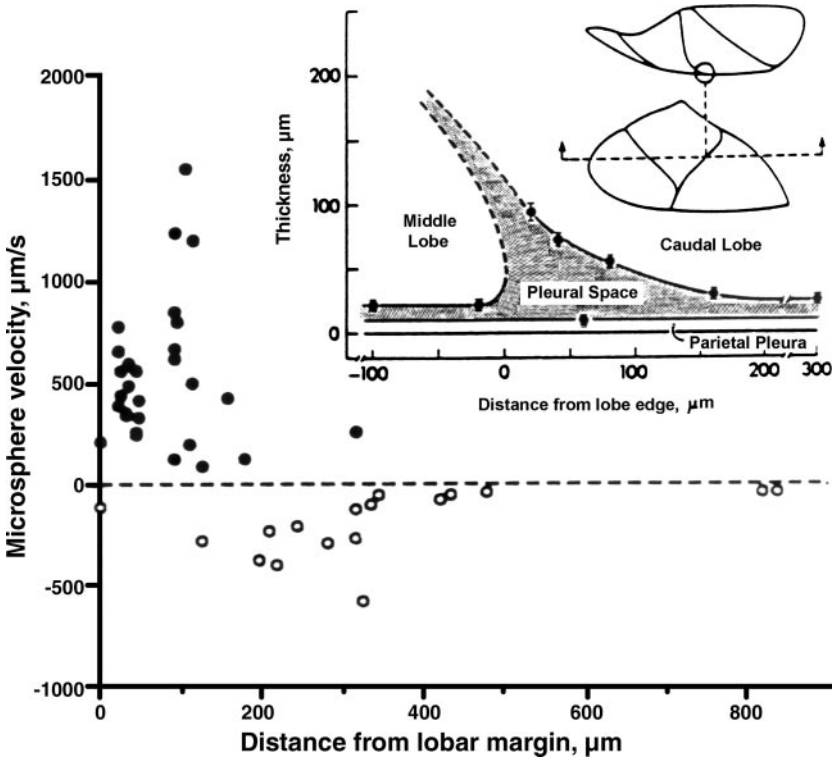

FIG. 5. Upward (positive) and downward (negative) velocity of 6-μm fluorescent latex microspheres at lobar margins caused by cardiogenic motion. *Inset* shows profile of pleural space measured in the vicinity of a lobar margin by light microscopy in the rabbit. Note that microspheres moved upward along the lobar margin where the pleural space was relatively wide and downward where the pleural space was narrow. [Modified from Lai-Fook (97) and Wang and Lai-Fook (201).]

C. Transverse Flows: the Ventilatory Pump

Two studies using fluid mechanics to describe the flow in thin channels have modeled recirculation of pleural liquid by ventilatory motion. In the first study (54), a ventilatory pump moves liquid from lobar margins to the flat costal surfaces in a direction that is opposite to what occurs under apneic conditions due to the static pressure gradient (Fig. 2). The analysis showed that pleural liquid thickness (h) on the flat costal surface is related to lung velocity amplitude (U) and the costal surface-to-lobar margin pressure difference (ΔP)

$$h = (T/\Delta P)(\nu U/T)^{2/3} \quad (3)$$

where T is membrane tension. The prediction from *Equation 3* was reproduced in a balloon-in-cylinder model of the pleural space in conjunction with vertical strings to simulate lobar margins. The thickness of the model's pleural space increased with velocity amplitude and decreased with the pressure difference. This behavior is qualitatively consistent with in vivo studies that showed pleural liquid thickness to increase with ventilation (Fig. 4*A*).

In the other study (96a), the change in thickness of a fluid layer between two membranes with a local decrease in spacing was studied in response to relative sliding of the membranes. The presence of the decreased spacing increases the local fluid pressure, which causes the membranes to separate into a more uniform spacing. The results suggest a mechanism based on ventilation-induced shear stress to prevent contact between the two pleural surfaces as the surfaces approach each other.

D. Fluid Volume Homeostasis

Homeostasis in pleural liquid volume considered within the context of viscous flow concepts (97) comes about by a matching of the microvascular filtration rate to the flow within the pleural space. In the steady state, microvascular filtration or pleural liquid flow equals the outflow by lymphatic stomata. Pleural liquid flow that results from gravity, for example, is related to pleural liquid thickness through the viscous pressure losses that balance the net driving pressure (*Eq. 2*). Any change in filtration would result in a new equilibrium value for pleural liquid thickness and pleural liquid volume (100). This concept of homeostasis of pleural liquid volume based on flow is different from that based on hydrostatics (1, 2). According to homeostasis based on hydrostatics, pleural capillaries absorb pleural fluid until there is contact between the two pleural surfaces, at which point pleural liquid pressure attains a hydrostatic equilibrium and a minimal pleural liquid volume is reached.

The gravity-induced drainage of pleural liquid downward in the pleural space also ensures that any excess liquid accumulates in the most dependent part of the pleural space, which is the dependent part of the costophrenic sulcus forming the zone of apposition of the rib cage to the diaphragm (119). This excess fluid does not directly participate in lubrication of the lung surface and has no effect on regional ventilation.

V. MICROVASCULAR EXCHANGE

A. Pleural Anatomy and Blood Supply

The parietal and visceral pleura have a common origin during development (75). The structure of pleura is that of extracellular matrix, including collagen and elastic fibers (157), covered by a layer of mesothelial cells. Mediastinal pleura and pericardium are continuous with parietal and visceral pleura and in part are free standing. The free-standing parts have two layers of mesothelial cells.

McLaughlin et al. (116) classified mammals into three groups according to their visceral pleural thickness. Those with thick pleura include the pig, sheep, and cow. Those with intermediate thickness include the horse and human. Those with thin pleura include the mouse, rat, rabbit, cat, and dog. In the sheep, the visceral pleural thickness ranges from 25 μm in the cranial regions to 85 μm on the diaphragmatic surface (28). This spatial variation might be related to movement with breathing (186) in view of the cranial-caudal gradient in lung-chest relative velocity measured in rabbits (Fig. 4*B*). In sheep, the parietal pleura is of fairly constant thickness, 23 μm (29). In humans it is 30–40 μm (167).

The blood supply to the visceral pleura depends on its thickness group. The thin visceral pleura of the small mammals have a pulmonary circulation. Intermediate and thick visceral pleura of the larger mammals have a bronchial (systemic) circulation (65). The drainage of the bronchial circulation occurs via the veins of the pulmonary circulation (38). In the sheep, the blood supply is located 10–15 μm from the parietal pleural surface (29).

B. Transport Equations: Starling and Solute Flux Equations

Pleural liquid originates from pleural capillaries through the normal processes of microvascular filtration, similar to those that occur in other organs (34, 185, 190). Transport of pleural liquid and protein occurs across two barriers, the capillary endothelium in series with the pleural interstitium (membrane). The location of the capillary within the pleural membrane in relation to the pleural

space is illustrated schematically in Figure 6. As in other organs, the endothelium provides the major flow resistance and restriction to protein. However, the relative contribution of the interstitium to the overall barrier properties is still debated. Pleural membrane transport properties are summarized within a framework of two phenomenological equations, the Starling equation and the solute flux equation. Both equations are commonly used to describe the transport of liquid and solutes across biological membranes (60). The transport constants of the two equations derived for the two-membrane system are used to separate the contribution of the pleural interstitium from the combined endothelium-interstitial barrier properties.

1. The Starling equation

The Starling equation (184) relates the filtration rate (Q_b) across the capillary endothelial barrier in series with the pleural membrane (interstitium) to the hydrostatic (P) and protein (colloid) osmotic pressure (π) difference between capillary blood and pleural liquid

$$Q_b = LA[(P_c - P_{pl}) - \sigma_o(\pi_c - \pi_{pl})] \quad (4)$$

where subscripts c and pl refer to microvasculature and pleural liquid, respectively, L is hydraulic conductivity, A is surface area, and σ_o is the reflection coefficient to protein of the combined endothelial-interstitial barrier. LA is the filtration coefficient.

2. The solute flux equation

The mass flux of a solute (Q_s) across the endothelial-interstitial barrier is given by the solute flux equation (60, 190)

$$Q_s = C_m(1 - \sigma_d)Q_b + DA(C_c - C_{pl})/l \quad (5)$$

where C_m is the mean solute concentration in the membrane, σ_d is the solute drag reflection coefficient, D is apparent diffusion coefficient, A is total membrane surface area, l is membrane thickness, and C is solute concentration. For the flow of a single solute, σ_o equals σ_d (173). The first term on the right-hand side of *Equation 5* describes the solute flux due to bulk flow given by the Starling equation (*Eq. 4*), while the second term describes the solute flux due to diffusion.

C. Hydraulic Conductivity, Reflection Coefficient, and Diffusive Permeability

1. Hydraulic conductivity

Since the flow across the endothelium and interstitium are in series, their flow resistances (inverse of conductivity) add (assuming $\sigma_o\Delta\pi = 0$ in *Eq. 4*)

$$1/L_o = (1/L_c) + (1/L_i) \quad (6)$$

where subscripts o, c, and i refer to overall, endothelial, and interstitial parameters, respectively.

Table 3 lists values of hydraulic conductivity (L) measured for the endothelial-interstitial barrier of the visceral pleura of dog lungs and values of visceral pleura, parietal pleura, mediastinal pleura, pericardium, and diaphragm measured in a variety of species. The pericardium and diaphragm are considered alongside the other pleural membranes because they are parts of a continuous sac lining the chest cavity, while the mesentery has morphological and transport properties similar to pleura.

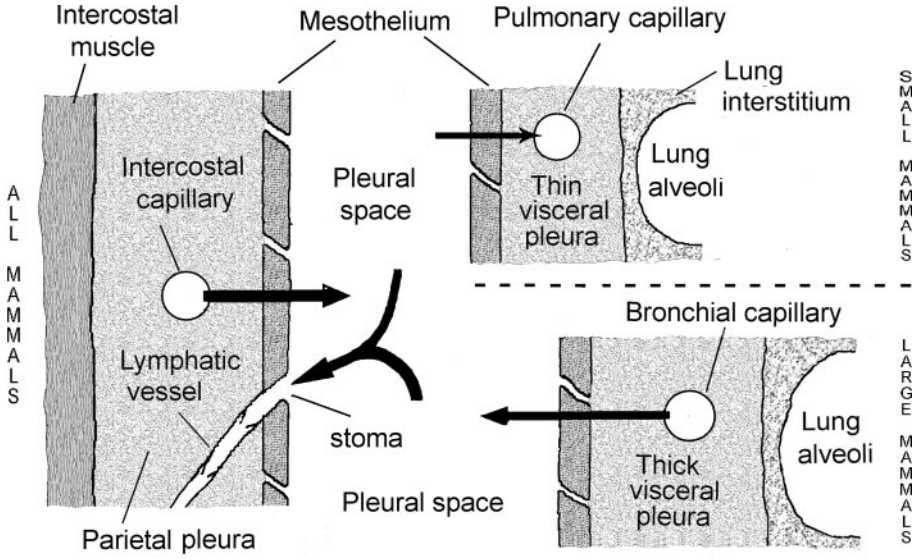

FIG. 6. Schematic diagram of the pathways for normal pleural liquid turnover. In all mammals, pleural liquid is mainly a filtrate from capillaries in the parietal pleura lining the chest wall (*left*). Arrows indicate direction of flow. In large animals with thick visceral pleura, some pleural liquid is filtered from the bronchial capillaries of the visceral pleura lining the lung (*bottom right*). In small animals with thin visceral pleura, a small amount of pleural liquid might be reabsorbed by pulmonary capillaries (*top right*). Drainage of pleural liquid from the pleural space occurs via lymphatic stomata in the parietal pleura. The pleural space, visceral pleura, and alveoli are thicker in large animals than in small animals.

TABLE 3. *Hydraulic conductivity*

Tissue	Species	Thickness, μm	*L*	*K*	Reference Nos.
Visceral pleura	Sheep	80*	1.6	1.3	92
Visceral pleura	Dog	15†	39	5.9	164
Parietal pleura	Dog	15†	190	29	164
Parietal pleura	Dog	15†	2.6	0.38	153
Parietal pleura (in situ)	Dog	15†	0.4	0.06	154
Parietal pleura (in situ)	Dog	15†	0.3	0.045	155
Parietal pleura (in situ)	Rabbit	13‡	0.6	0.078	155
Mediastinal pleura	Pig	130	20	21	162
Pericardium	Human	550	0.75	4.1	69
Pericardium	Dog	150	1.6	2.4	69
Pericardium	Rabbit	30	2.8	0.85	165
Pericardium	Dog	150	3.0	4.5	165
Pericardium	Pig	400	0.4	1.7	217
Pericardium	Rabbit	32	0.6	0.2	145
Diaphragm	Rat	600	0.4	2.4	143
Mesentery	Rabbit	32	90	27	163
Capillary/visceral pleura	Dog		0.5		14
Capillary/visceral pleura	Dog		0.03§		64
Capillary/visceral pleura	Dog		1.1		93
Capillary/visceral pleura	Dog		0.57		94
Capillary/visceral pleura	Dog		0.50		95
Single capillaries	Many	1	0.1–6	0.001–0.06	121

L, flow (cm^3/s) per unit ΔP (cmH_2O) per unit surface area (cm^2), expressed in 10^{-6} cm · s^{-1} · cmH_2O^{-1}; *K*, *L* × thickness (cm), 10^{-8} cm^2 · s^{-1} · cmH_2O^{-1}. * Data from costal part of caudal lobe (28). † Data from Payne et al. (164). ‡ Data from Lai-Fook and Kaplowitz (101). § Order of magnitude estimate.

Studies by Kinasewitz and co-workers (164) showed that the overall conductivity measured in the whole lung was much smaller than interstitial conductivity measured in vitro (94). Thus the endothelial conductivity is almost equal to the overall conductivity, and the resistance to flow from the capillaries to the pleural space is predominantly caused by the endothelium (*Eq. 6*). Almost the entire pressure drop occurs across the endothelium, and thus interstitial pressure is virtually equal to pleural liquid pressure.

Membrane thickness varies from 15 μm for the dog pleura (101) to ~80 μm for the sheep visceral pleura (28) and giant rabbit pericardium (42, 43) to 130–400 μm for the pig mediastinal pleura (162) and pericardium (217). Therefore, for comparison purposes, the appropriate measure of conductivity is $K = L \times l$. *K* is then the flow per unit area per unit pressure gradient ($\Delta P/l$), whereas *L* is flow per unit area per unit pressure difference. In the in vitro studies, a piece of tissue was mounted between two chambers in an Ussing-type apparatus. The flow of Ringer solution across the membrane was measured in response to a hydrostatic pressure difference. Measurements of visceral and parietal pleura required stripping the membrane from the lung and rib cage, respectively, a procedure that has been criticized on the grounds that it causes trauma to the tissue. Mediastinal pleura, pericardium, diaphragm, and mesentery are free standing, and no stripping was required for the in vitro studies. In in situ studies, a capsule was bonded to a pleural window made by dissection of intercostal muscle and endothoracic fascia. Flow across the pleura into the capsule from the pleural space was measured as intracapsular pressure was varied.

In general, the results of hydraulic conductivity (*K*) fall into two groups: values of relatively high conductivity ($0.2–29 \times 10^{-8}$ $cm^2 \cdot s^{-1} \cdot cmH_2O^{-1}$) and values of an order of magnitude smaller conductivity ($\sim 0.05 \times 10^{-8}$ $cm^2 \cdot s^{-1} \cdot cmH_2O^{-1}$). The high conductivity values were associated with in vitro measurements of parietal (164, 153), visceral (92), and mediastinal pleura (162), diaphragm (143), and pericardium (69, 145, 165, 217). Parietal and visceral pleural membranes that were stripped from the chest wall and lung, respectively, produced values similar to those of free-standing mediastinal and pericardial membranes. Thus trauma caused by stripping was unlikely the reason for the high conductivity values. A similar conclusion applies to the effect of stripping on reflection and diffusion coefficients (see below). Similar values for hydraulic conductivity were obtained for pig pericardium with mesothelial layers removed (217) and for dog (69, 165), human (69), and rabbit (165) pericardium with intact mesothelium. Thus the mesothelial layers were not the major contributor to the measured conductivity.

The low hydraulic conductivity values were associated with the in situ studies. In these studies, the resistance to flow into the capsule might have been artifactually increased by the thinning of the pleural space beneath the capsule as the negative pressure in the capsule was

transmitted to the lung. The lower parietal pleural conductivity ($0.05–0.08 \times 10^{-8}$ $cm^2 \cdot s^{-1} \cdot cmH_2O^{-1}$) measured in situ was about the same as the highest value measured for the endothelium ($0.001–0.06 \times 10^{-8}$ $cm^2 \cdot s^{-1} \cdot cmH_2O^{-1}$) and indicated a significant pressure drop across the interstitium. This behavior was supported by parietal interstitial pressure measured by cannulas and micropuncture that showed a 2–6 cmH_2O interstitial-to-pleural liquid pressure difference (129, 150); that is, 10–20% of the total pressure drop was assigned to the interstitium (133).

In summary, the results of the conductivity studies showed that most (>80%) of the flow resistance of the pleural endothelial-interstitial barrier was associated with the capillary endothelium.

2. Reflection coefficient

The protein osmotic pressure exerted across the capillary endothelium and pleural interstitium depends on the overall reflection coefficient of the two components. From the Starling equation (*Eq. 4*) with $\Delta P = 0$ and A constant

$$1/(L_o\sigma_o) = 1/(L_c\sigma_c) + 1/(L_i\sigma_i) \quad (7)$$

With the use of *Equation 6*

$$\sigma_o/\sigma_c = (1 + L_c/L_i)/[1 + (L_c/L_i)(\sigma_c/\sigma_i)] \quad (8)$$

Table 4 lists albumin reflection coefficients of pleural membrane (interstitium) measured in several species. The measured interstitial reflection coefficients (0–0.5) are much smaller than those measured for the capillary endothelial-interstitial barrier (0.61–0.93) and for single capillaries (0.9). Thus, on this basis, the endothelium is the primary barrier to the transport of protein into the pleural space.

TABLE 4. *Albumin reflection coefficients (σ)*

Tissue	Species	σ	Method	Reference Nos.
Parietal pleura	Dog	0	Excised tissue	164
Parietal pleura	Dog	0.11	Excised tissue	153
Parietal pleura	Dog	0.4	In situ	155
Parietal pleura	Rabbit	0.3	In situ	155
Mediastinal pleura	Pig	0.02–0.05*	Excised tissue	162
Pericardium	Rabbit	0.42	Excised tissue	165
Pericardium	Rabbit	0.1–0.3†	Excised tissue	145
Diaphragm	Rat	0.1–0.5†	Excised tissue	143
Mesentery	Rabbit	0.02–0.14*	Excised tissue	163
Capillary/visceral pleura	Dog	0.61–0.93	In situ: lung in bag	94
Capillary endothelium	Many	0.9	Single capillaries	121

* Reflection coefficient increased with flow. † Reflection coefficient decreased with albumin concentration measured using flow-independent sieving ratio. All other studies used osmotic transient method.

Because the reflection coefficient of the endothelium is greater than that of the interstitium, for any value of L_c/L_i, the overall reflection coefficient is less than the endothelial reflection coefficient (*Eq. 8*). *Equation 8* shows that for $L_c \ll L_i$, σ_o tends to σ_c, and for $L_c \gg L_i$, σ_o tends to σ_i. Thus a small interstitial reflection coefficient always reduces the overall reflection coefficient of the endothelial-interstitial barrier from the value for the endothelium. For example, for an interstitial reflection coefficient of 0.2, endothelial-to-interstitial conductivity ratio of 0.1 and endothelial reflection coefficient of 0.9, the overall reflection coefficient is reduced to 0.68.

Reflection coefficients near zero were measured in in vitro studies of both stripped dog parietal pleura (153, 164) and free-standing pig mediastinal pleura (162). Values of reflection coefficient measured in rat diaphragm (143) and rabbit pericardium (145) decreased from 0.3–0.5 with Ringer solution to 0.15 with an albumin concentration of 1–2 g/dl. In the mesentery (163) and mediastinal pleura (162), reflection coefficients (0.02–0.14) increased with flow. Thus differences in both albumin concentration and flow might be responsible for the variability in the reflection coefficients among the studies.

In the in situ studies (155), the albumin reflection coefficients of the parietal pleural interstitium, 0.3 in the dog and 0.4 in the rabbit, were greater than the in vitro measurements. These higher values would lower the overall reflection coefficient of the endothelial-interstitial barrier (*Eq. 8*), reduce the protein osmotic pressure gradient opposing filtration, and increase the net filtration pressure into the pleural space. Applied to the visceral pleura, a small interstitial reflection coefficient would reduce any reabsorption from the pleural space.

In experiments using intercostal capsules bonded to parietal pleura of rabbits (155), the transport of labeled macromolecules from pleural liquid to the parietal pleural capsule was consistent with two sets of pores in the parietal pleura, 8.5 and 19 nm. Based on the theory of restriction of solutes through cylindrical pores (60), the smaller pore is consistent with an interstitial reflection coefficient of 0.4, similar to the value found in rabbit lung interstitium (195) and rat diaphragm (143) for low albumin concentrations.

In summary, all studies showed reflection coefficients that were smaller for the interstitium than for the endothelium. Thus restriction of protein by the pleural capillary endothelial-interstitial barrier was largely associated with the endothelium.

3. Diffusive permeability

Table 5 summarizes albumin permeability and diffusion coefficients measured in a variety of tissue membranes of several species. Permeability is the parameter required to estimate the relative contribution of pleural interstitium and capillary endothelium to the overall endothelial-interstitial barrier. Permeability (Pe) is equal to diffusion coefficient divided by membrane thickness (D/l). The overall permeability (Pe_o) is related to interstitial (Pe_i) and endothelial (Pe_c) permeability, with the assumption of zero bulk flow and constant surface area (A, *Eq. 5*), as follows

$$1/Pe_o = 1/Pe_c + 1/Pe_i \quad (9)$$

If interstitial permeability were much greater than endothelial permeability, the overall permeability would almost equal endothelial permeability, and the major diffusive resistance would be associated with the capillary endothelium. That the endothelium dominates the overall barrier to diffusion was supported by permeability values of the capillary-interstitial barrier of the visceral pleura measured in perfused dog lungs (94, 95) that was two orders of magnitude smaller than that of visceral pleural interstitium (164). In contrast, the permeability of parietal pleura measured in rabbits by intercostal capsules was lower (155) than that measured for the endothelial-interstitial barrier of dog visceral pleura (94, 95). This implied that the pleural interstitium contributed the major resistance to the diffusion of albumin across the endothelial-interstitial barrier.

Almost all data of the in vitro studies (Table 5) support a relatively small contribution of interstitial diffusive resistance to the overall diffusive resistance. Because the pleural membrane thickness varies considerably among species, diffusion coefficient $D = Pe \times l$ is the appropriate parameter for comparison among species. The measured diffusion coefficients are usually associated with the extracellular matrix because nearly similar values were obtained from a wide range in tissue thickness (30–600 μm). In contrast, diffusive permeability measured in pericardium has been attributed to the mesothelium because scraping the mesothelium from the tissue increased permeability 10-fold (43). However, the scraping might also have increased tissue permeability.

In vitro values of albumin diffusion coefficient (0.4–22 $\times 10^{-8}$ cm^2/s) were two orders of magnitude greater than the in situ values (2–12 $\times 10^{-10}$ cm^2/s). Diffusion coefficients might be somewhat greater in the in vitro studies because isolated tissue immersed in solution always increases hydration spontaneously by ~50% (56, 143).

Diffusion of albumin in mediastinal pleura (162) and rat diaphragm (143) increased with concentration. This behavior is consistent with the reduced reflection coefficient measured with an increase in albumin concentration and implies an enhanced absorption of interstitial albumin under conditions of increased microvascular permeability.

In summary, the results of most studies showed that the diffusive resistance to protein was much smaller for the interstitium than for the endothelium. This indicated that the major barrier to diffusion was associated with the endothelium.

D. Pleural Filtration Pressure and Filtration and Absorption Rates

1. Pleural filtration pressure

Whether the Starling force balance across the pleural microvascular barrier favors filtration or reabsorption is still debated, with the evidence strongly in favor of an overall net filtration into the pleural space. There is a general consensus that pleural liquid is a microvascular

TABLE 5. *Albumin permeability and diffusion coefficients*

Tissue	Species	Thickness, μm	Pe, 10^{-6} cm/s	D, 10^{-8} cm^2/s	Reference Nos.
Visceral pleura	Dog	15*	34	4.4	164
Parietal pleura	Dog	15*	130	20	164
Parietal pleura	Dog	15*	10	1.5	153
Parietal pleura (in situ)	Dog	15*	0.8	0.12	154
Parietal pleura (in situ)	Rabbit	13†	0.15	0.02	155
Mediastinal pleura	Pig	130	2.3	3	162
Pericardium	Rabbit	30	73	22	165
Pericardium	Rabbit	32	1.3	0.4	144
Pericardium	Rabbit	70	0.9	0.63	42, 43
Diaphragm	Rat	600	0.75	6	143
Capillary/visceral pleura (lung)	Dog		2.4		94
Capillary/visceral pleura (lung)	Dog		4.3		95

Permeability coefficient (Pe) = diffusion coefficient (D)/thickness. * Data from Payne et al. (164). † Data from Lai-Fook and Kaplowitz (101).

filtrate from the parietal pleural capillaries. The debate centers on the contribution of visceral pleural capillaries and interstitial lymphatics to the absorption of pleural liquid and protein.

Table 6 shows the values of the Starling forces used to evaluate the net filtration pressure published in several reviews (18, 133, 186) and other sources (100). The values for parietal pleura and visceral pleura are listed separately. Hydrostatic pressures in the microvasculature (capillary) and pleural space are given for midlung height. Since capillary pressure varies as 1 cmH_2O/cm height, whereas pleural pressure is uniform for the normal prone posture, the hydrostatic pressure difference across the barrier would be reduced in nondependent regions and increase in dependent regions.

The effective protein osmotic pressure difference across the endothelial-interstitial barrier, $\sigma_o(\pi_c - \pi_{pl})$, favoring plasma retention of liquid varies from 23 cmH_2O in sheep (186) and dog (18) to 10–13 cmH_2O in the rat (100) and rabbit (133). The value of σ_o used (~0.9) was appropriate for the endothelium (121). The smaller values of protein osmotic pressure difference across the endothelial-interstitial barrier are mainly due to relatively high values of protein colloid osmotic pressure for pleural liquid coupled with relatively low values for blood plasma measured in the smaller mammals. These estimates of protein osmotic pressure difference are maximal, since any significant reflection coefficient and hydraulic conductivity for the interstitium would reduce the overall reflection coefficient and osmotic pressure difference for the total barrier (see sect. v*C2*).

The parietal pleura has a systemic circulation, and its capillary pressure ranges from 17 to 34 cmH_2O. Pleural pressure at end-expiratory lung volume varies from −2 to −4 cmH_20 (1, 2). The hydrostatic pressure difference ($P_c - P_{pl}$) favoring filtration has a range of 21 cmH_2O in the rabbit (133) to 31 cmH_2O in the rat (100), which together with a 10–23 cmH_2O osmotic pressure difference opposing filtration, produces a net filtration pressure $[(P_c - P_{pl}) - \sigma_o(\pi_c - \pi_{pl})]$ of 8–21 cmH_2O. These values are minimal estimates since respiration reduces the pleural pressure below the values used at end-expiration.

The forces favoring filtration or reabsorption in the visceral pleura are arguable because the blood supply to the visceral pleural capillaries has a systemic source in the larger mammals, including humans, but a pulmonary source in smaller mammals (116). Although a systemic (bronchial) circulation supplies the visceral pleura of the larger mammals, the bronchial arteries drain into the pulmonary veins (65) and the magnitude of the pressure in the visceral pleural capillaries is somewhat uncertain. Accordingly, in the visceral pleura, a net filtration pressure similar to that for the parietal pleura (9 cmH_2O) is calculated for a systemic source in sheep (186) and for a pulmonary source in the rat (11 cmH_2O). In contrast, a zero or net absorptive pressure is calculated for a pulmonary source in the sheep (186), dog (18), and rabbit (133). However, the magnitude of the net absorptive pressure (~0 to −4 cmH_2O) into the visceral pleura is much smaller than the net filtration pressure (8–21 cmH_2O) from the parietal pleura, which by itself indicates an overall net filtration into the pleural space of all species. The lower pleural pressure with breathing would reduce the small absorptive pressure in the visceral pleura estimated at end-expiratory lung volume (sheep and rabbit).

Net filtration pressure by itself is not sufficient to determine whether net filtration or absorption occurs from the parietal and visceral pleural membranes because filtration is the product of hydraulic conductivity and net filtration pressure (*Eq. 4*). Given about the same hydraulic conductivity for visceral and parietal pleura (Table 3) and the same blood flow in both pleura, the much larger net filtration pressure for the parietal pleura compared with a smaller net absorptive pressure for the visceral pleura would support an overall net microvascular filtration into the pleural space. An exception in the data (Table 3) is the parietal pleural hydraulic conductivity measured with intercostal capsules (154, 155) that is 1–2 orders of magnitude smaller than that measured in the other studies and similar to that of the visceral pleural endothelium-inter-

TABLE 6. *Filtration pressures (cmH_2O) for parietal and visceral pleura*

Species	P_c	P_{pl}	$P_c - P_{pl}$	σ_o	π_c	π_{pl}	$\sigma_o(\pi_c - \pi_{pl})$	Net	Reference Nos.
Parietal pleura									
Sheep	28	−9	37	0.9	30	4	23	14	186
Rabbit	17	−4	21	0.8	25	8	13	8	133
Rat	34*	−3	37	0.9	20	9	10	21	100
Visceral pleura									
Sheep (systemic)	23	−9	32	0.9	30	4	23	9	186
Sheep (pulmonary)	11	−9	20	0.9	30	4	23	−3	186
Rabbit	10	−4	14	0.7	28	8	14	0	133
Rat	14	−3	17	0.9	17	10	6	11	100
Dog	10	−9†	19	0.9	29	3	23	−4	18

Net = $[(P_c - P_{pl}) - \sigma_o(\pi_c - \pi_{pl})]$. π_c is derived from protein concentration using Landis and Pappenheimer's equation (106). * Data from Bohlen et al. (45). † Data are mean pressure during breathing cycle (18).

stitial barrier. However, the low parietal pleural conductivity is offset by a relatively high interstitial reflection coefficient (Ref. 155; Table 4) that would reduce the osmotic retention by plasma and increase filtration.

The absorption of water from the pleural space into the lung visceral pleural capillaries (93) was observed with the appropriate manipulation of the Starling forces *(Eq. 4)*. In contrast, with pulmonary edema, lung edema crossed the visceral pleura into the pleural space (52, 213) because the pressure in lung interstitium is above the pleural pressure (41, 68, 71, 72).

Physiological studies have provided evidence that the source of pleural liquid is the systemic capillaries of the parietal pleura. Mellins et al. (120) elevated systemic and pulmonary venous pressure separately or together in dogs and found that the accumulation of pleural liquid was much larger with systemic than with pulmonary venous hypertension. Further evidence for a parietal source of pleural liquid is that the pleural effusions produced by an increased pulmonary venous pressure in dogs were derived from pulmonary edema and not from the capillary hypertension of the visceral pleura (31).

Other physiological evidence supports the conclusion that there is an overall net microvascular filtration into the pleural space. First, tracer studies showed that pleural liquid and solute absorption were primarily associated with lymphatic stomata on the parietal pleural surface with little evidence for visceral pleural absorption (28, 29, 40, 50, 58, 59, 206). Second, imaging studies indicated that lymphatic absorption increased toward the caudal regions where the lymphatic stomata are concentrated (152). Third, anatomic and morphological studies in sheep showed that the microvessels in the parietal pleura were located 15 μm from the pleural surface (29), whereas the microvessels in the visceral pleura were located much deeper (20–50 μm; Ref. 28). Accordingly, in sheep hydraulic conductance from the pleural space to the microvessels would be less in the visceral than in the parietal pleura, and filtration from or reabsorption into the visceral pleural capillaries would be inhibited. Thus pleural anatomy, at least in sheep, supports the physiological evidence that pleural liquid filtration occurs via the parietal pleura (186). However, in the smaller mammals with a visceral pleura similar in thickness to the parietal pleura, any reabsorption of pleural liquid into visceral pleural capillaries with a high reflection coefficient would concentrate pleural liquid protein and perhaps account for the greater protein concentration in the smaller mammals (see sect. VI, Table 8, Fig. 7). Finally, reabsorption of pleural liquid by the lung interstitium, though possible, is unlikely in view of subpleural interstitial pressures that were slightly (1 cmH_2O) above the pleural pressure (41, 68, 71, 72). These results contrast to a negative lung interstitial pressure of -10 cmH_2O measured in situ at locations 200 μm below the pleural surface (134, 135).

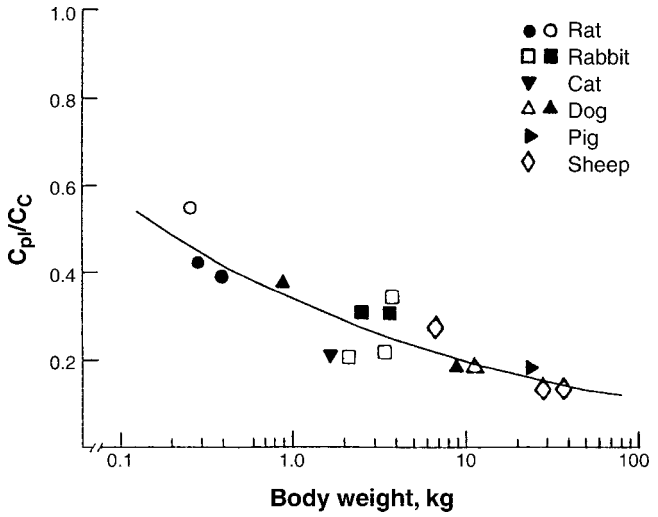

FIG. 7. Ratio of total protein concentration in pleural liquid to that in plasma (C_{pl}/C_c) versus body mass (M) in several species. Note that C_{pl}/C_c decreases with body mass, according to the allometric relationship (solid line): $C_{pl}/C_c = 0.34\ M^{-0.23}$ ($R^2 = 0.78$, $n = 16$, $P = 7 \times 10^{-6}$). [Modified from Lai-Fook (97).]

Interstitial protein concentration measured in the parietal pleura of rabbits by implanted wick catheters (148) was 2.6 g/dl, somewhat smaller than that in pleural liquid (3.1 g/dl). The calculated interstitial-to-pleural liquid protein osmotic pressure difference was 3.5 cmH_2O or 27% of the total difference between the capillary and pleural liquid (13 cmH_2O). The interstitial-to-pleural liquid hydrostatic pressure difference measured by micropuncture was 1.8 cmH_2O (129). These differences in protein osmotic pressure assigned to the parietal pleural membrane can be questioned because of the uncertainty of the location of the wick used for collecting the interstitial liquid (18). In spite of the objections, the small differences in hydrostatic and protein osmotic pressures do not substantially change the overall net filtration pressures and thus do not invalidate the assumption that protein concentration of pleural liquid largely reflects that of the microvascular filtrate.

In summary, the pathways for normal pleural liquid turnover are illustrated schematically in Figure 6. Pleural liquid is derived mainly from capillaries in the parietal pleura lining the chest wall of all mammals. Some pleural liquid is filtered from bronchial capillaries in the thick visceral pleura of large mammals. Pleural liquid is removed by lymphatic stomata in the parietal pleura. A small reabsorption of pleural liquid might occur into the pulmonary capillaries of the thin visceral pleura of the smaller animals.

2. Filtration and absorption rates

Table 7 summarizes the pleural liquid filtration and absorption rates estimated in several species. The esti-

TABLE 7. *Pleural liquid filtration and absorption rates*

Species	Rate, ml · h^{-1} · kg^{-1}	Method	Reference Nos.
Rabbit	0.017	Catheter drain	48
Dog	0.020	Tracer kinetics and lymph clearance	124
Dog	0.019	Imaging of tracer in ~1 ml hydrothorax	152
Sheep (awake)	0.01	Tracer kinetics into pleural space from blood	212
Rabbit	0.22*	2 ml hydrothorax	136
Rabbit	0.22*	1 ml hydrothorax	15
Dog	0.57*	12 ml/kg hydrothorax	188
Dog	0.47‡	12 ml/kg hydrothorax	188
Sheep (anesthetized)	0.02†	Tracer in lymph, 10 ml/kg hydrothorax	212
Sheep	0.22*	10 ml/kg hydrothorax	212
Sheep	0.28*	10 ml/kg hydrothorax	52
Human	0.36*	Heart failure/malignant effusions	187
Human	0.11*	Effusions	110

* Absorption rate was calculated from the volume of hydrothorax recovered. † This value proved to be a gross underestimate by a subsequent study (52). ‡ Filtration rate.

mated filtration rate measured without hydrothoraces scales approximately to body weight. In unanesthetized sheep, the appearance in pleural liquid of tracer ^{125}I-albumin injected into the blood produced a protein filtration rate of 0.01 ml·h^{-1}·kg^{-1} (212). Somewhat greater values (0.02 ml·h^{-1}·kg^{-1}) for pleural filtration have been estimated in the dog (124, 152) and rabbit (48). In contrast, studies using large hydrothoraces produced much higher pleural liquid absorption rates (0.11–0.57 ml·h^{-1}·kg^{-1}) in sheep (50, 212), rabbits (15, 136), dogs (188), and humans (110, 187). Thus, with large hydrothoraces, absorption of pleural liquid can increase 10- to 30-fold above the normal turnover rate (18, 50, 125, 126, 133, 186). Accordingly, absorption of large hydrothoraces is not a reliable measure of normal filtration into the pleural space or of the normal turnover rate of pleural liquid.

The volume of pleural liquid divided by the filtration rate provides an estimate of the pleural liquid transit time, that is, the time required to turnover the entire pleural liquid volume. From values provided in Tables 2 and 7, the turnover time for pleural liquid is 10–13 h for rabbits and sheep.

E. Regional Absorption, Role of Lymphatics, and Regional Filtration

1. Regional absorption

Regional absorption of pleural liquid has been studied by histological identification and external imaging of tracers injected into the pleural space. Anatomical studies showed that absorption sites via lymphatic stomata are concentrated in the ventral-caudal and dorsal-caudal regions of the parietal pleura of the rib cage in sheep (29, 115) and rabbits (197) and in the diaphragm of rabbits (151). Tracer studies showed that the visceral pleural lymphatics do not participate in pleural liquid absorption (50, 206). The concentration of lymphatic stomata in the caudal regions of the pleural space was supported by imaging studies in dogs, which showed a lower absorption rate of radioactive tracer from cranial regions than from caudal and mediastinal regions (152). The distribution of lymphatic stomata concentrated in the intercostal spaces rather than on the rib surfaces (29) was supported by fluorescent studies that showed a greater absorption in the intercostal muscle than in the rib (206).

2. Role of lymphatics

Lymphatic drainage from the pleural space occurs via the stomata in the parietal pleura (29, 181). The ultrastructure of stomata has been described in the parietal pleura (108, 197) and the peritoneum (108). The mechanism by which lymphatics absorb pleural liquid remains speculative. One model postulated that the pleural liquid pressure was set by the lymphatics and that the absorption rate was determined by the pressure-volume relationship of the pleural space (141). As the volume of the pleural space was reduced, the pleural liquid pressure and the pressure gradient for lymphatic absorption decreased. The pressure generated by parietal pleural lymphatics was estimated to be -7 cmH_2O relative to pleural pressure (138). This absorptive pressure for pleural lymphatics is below the mean values (~0 cmH_2O) measured in the intercostal pleural lymphatics of rabbits (149) and in other organs (179). However, the pressure associated with the absorption of liquid via lymphatics might be generated by cardiogenic and smooth muscle contractile oscillations in conjunction with unidirectional valves (146, 149, 179).

The postulate (130, 131) that an absorptive pressure in pleural lymphatics below the pleural liquid pressure determines the pleural liquid pressure seems unlikely based on the following considerations. First, the distribu-

tion of lymphatic stomata even where they are most concentrated is sparse. In sheep (29), one stoma of 1–3 μm diameter is found per 25 $\times$ 25 μm surface area. In the rabbit diaphragm (151), one stoma is found per 60 $\times$ 60 μm surface area. The primary mechanism for fluid absorption into lymphatic stomata from adjacent sites is redistribution of pleural liquid by ventilatory and cardiogenic motion, not a flow driven by a difference in hydrostatic pressure. Second, lymphatic stomata are concentrated in the caudal regions of the pleural space with few in the cranial regions, a spatial distribution that is not matched by a cranial-to-caudal difference in pleural liquid pressure.

Since the absorption rate of hydrothoraces is considerably greater than the normal turnover rate of pleural liquid, experiments using the absorption of hydrothoraces comprising saline or plasma (136) do not provide reliable evidence for lymphatic absorption under normal conditions. Indeed, the results of these experiments proved to be not reproducible (19). These results are difficult to interpret because the changes in visceral pleural capillary filtration with protein concentration of the hydrothorax and in lymphatic absorption with the size of the hydrothorax are difficult to estimate. The concept that pleural lymphatics can concentrate protein does not have direct experimental support. The usual assumption based on data from other organs is that lymphatics do not restrict the passage of protein from interstitial liquid (34, 179).

3. Spatial variation in filtration

In contrast to the anatomic and physiological studies of the pleural liquid absorption sites, there is a paucity of studies of regional pleural liquid filtration. Fluorescence of Evan's blue-dyed albumin emitted from the parietal pleura of rabbits 6 h after injection into the circulation showed a cranial-caudal gradient in filtration (206). Albumin filtration was lowest at the cranial ribs and increased with rib number to reach a maximum at the seventh rib. This cranial-caudal distribution matched the regional distribution of lymphatic absorption sites measured anatomically (29, 197) and the regional distribution of an absorbed bolus (152). Perhaps not coincidentally, the cranial-caudal gradient in filtration matched that in pleural liquid thickness (Fig. 4*A*). The cranial-caudal gradient in protein filtration seems at odds with the uniform blood flow measured in the parietal pleura in dogs by radioactive microspheres (192).

VI. PLEURAL LIQUID PROTEIN CONCENTRATION

A. Effect of Body Size, Vascular Pressure, Ventilation, and Regional Differences

The concentration of protein present in the pleural liquid is important for the following reasons. First, it is one of the variables in the Starling equation that determines filtration. Thus its changes with body size might indicate differences in filtration and absorption of pleural liquid. Second, changes in pleural liquid protein concentration with ventilation might indicate shear stress-induced changes in pleural membrane permeability. Third, regional changes in protein concentration might indicate regional changes in filtration.

1. Effect of body size

Table 8 lists values of pleural liquid-to-plasma (capillary) protein concentration ratio (C_{pl}/C_c) from several sources. Figure 7 is a plot of C_{pl}/C_c versus body mass.

TABLE 8. *Pleural liquid-to-plasma total protein concentration ratio*

Species	C_{pl}, g/dl	C_c, g/dl	C_{pl}/C_c	Weight, kg	Reference Nos.
Rat	2.5	6.4	0.39	0.45	137
Rat (WKY)	2.4	4.3	0.55	0.27	100
Rat (SHR)	2.0	4.8	0.42	0.30	100
Cat	1.4	6.5	0.21	1.7	137
Dog (pup)	2.3	6.0	0.38	0.8	137
Rabbit	1.33	6.2*	0.21	2.2	127
Rabbit	1.4	6.2*	0.23	3.5	177
Rabbit	1.9	6.2	0.31	2.3	137
Rabbit	2.0	6.2	0.32	3.5	207
Rabbit	2.3	6.6	0.34	3.5	205
Sheep (fetus)	1.7	3.4	0.50	3.5	49
Sheep (newborn)	1.5	5.5	0.27	7.7	49
Dog	1.1	5.8	0.18	9	137
Dog	1.06	6.0*	0.18	11	127
Pig	1.2	6.3	0.19	24	137
Sheep (adult)	0.88	6.2	0.15	27	50
Sheep (adult)	0.96	6.2	0.15	28	212

C_{pl}, pleural liquid concentration; C_c, plasma total protein concentration. * Data from Miserocchi et al. (137).

Experiments by Miserocchi et al. (137) in several mammalian species showed that C_{pl}/C_c decreased with an increase in animal size. In sheep, where the vascular supply to the visceral pleura is systemic rather than pulmonary, C_{pl}/C_c is ~0.15 (50, 212). This low C_{pl}/C_c value points to a microvascular barrier that is relatively impermeable to protein with a reflection coefficient approaching 1.

2. Effect of vascular pressure

The decrease in C_{pl}/C_c with animal size has been explained on the basis of a vascular-to-pleural difference in hydrostatic pressure that increases with animal size (137). This explanation is supported by two other observations. Studies in the spontaneously hypertensive rat and its normotensive control rat showed that C_{pl}/C_c was reduced in the hypertensive rat, consistent with a washdown effect caused by a higher microvascular pressure and greater filtration (100). A similar decrease in C_{pl}/C_c occurred in sheep with development from the fetus to adulthood as systemic vascular pressure increased with age (49).

An alternative explanation for the decrease in C_{pl}/C_c with animal size is that smaller mammals with a pulmonary blood supply to the visceral pleura have a small net absorptive pressure into the visceral pleural capillaries that would increase the protein concentration in pleural liquid. Another possibility is a change in pleural membrane permeability with body size (97).

3. Effect of ventilation

In vitro studies of pleural mesothelial cells in culture showed a viscous flow-induced increase in permeability (208). Accordingly, the question whether an increased ventilation-induced shear stress can increase pleural membrane permeability to albumin was addressed in both anesthetized and conscious rabbits (205). In the anesthetized rabbits, an increase in mechanical ventilation for 6 h resulted in an increase in C_{pl}/C_c measured using Evan's blue albumin injected into the circulation, consistent with an increased permeability. However, subsequent studies in conscious rabbits showed no change in pleural liquid protein kinetics or systemic arterial pressure between breathing either room air or a hypercapnic gas mixture that increased ventilation. Thus the studies in conscious animals did not confirm the increased permeability observed in anesthetized animals and cultured cells.

4. Regional differences

In the absence of effective interregional mixing, a consequence of a greater dependent microvascular pressure and filtration would be a lower pleural protein concentration in the dependent regions of the thorax. Such a behavior has been reported for pulmonary interstitial protein as measured in visceral pleural lymphatics (26) but not for parietal pleural lymphatics. Studies in hypertensive rats showed an increased pleural liquid thickness and lower protein concentration with a hypertension-induced increase in filtration (100). Thus the lower pleural liquid thickness in the cranial region (Fig. 4*A*) in conjunction with a lower protein filtration (206) suggests that a relatively small filtration and a relatively high pleural liquid protein concentration would be found in the cranial region.

B. Active Protein and Solute-Coupled Liquid Transport

1. Active protein transport

Studies (5, 42) reporting active transport of protein by mesothelial cell vesicles have challenged the view that the primary route of protein absorption from the pleural space is via lymphatic stomata. The anatomy of the mesothelial cell does not exclude such a mechanism (39, 199). In vitro permeability studies of rabbit pericardium showed a reduced diffusive transport of albumin and dextran with the vesicular inhibitor nocodazole (42). Subsequent studies in anesthetized rabbits suggested that the vesicular inhibitor nocodazole reduced the absorption of tracer albumin and dextran measured 3 h after injection into the pleural space (5). However, in the latter study, the effect of the inhibitor on macromolecular absorption from the pleural space was measured with a hydrothorax, a condition that increases the pleural liquid absorption 10-fold above normal (Table 7). Thus this method cannot provide reliable information for normal conditions. Recent attempts to reproduce the permeability studies in rabbit pericardium showed an increased diffusion and hydraulic conductivity by nocodazole (144, 145) rather than a reduced transport. Moreover, other studies showed an increased microvascular permeability in response to vesicular inhibitors (55, 172). Thus mesothelial transcytosis as a mechanism for pleural liquid protein transport does not yet have conclusive supporting evidence.

2. Active liquid absorption

Studies in anesthetized rabbits (16–18, 218–224) and in excised human (178) and sheep pleura (79, 178) provided indirect evidence of a solute-coupled liquid absorption from the pleural space. The results of these studies have been summarized in a recent review (18). In the in vitro studies, significant but small (~10%) increases in electrical resistance were measured in response to Na^+ and K^+ transport inhibitors. There is a need to relate these small changes in electric resistance to liquid transport. In the in vivo studies, decreases in the absorption

rate of pleural liquid containing Na^+ transport inhibitors were extrapolated from values of the absorption rate with 0.5–5 ml hydrothoraces. A limitation of this approach is that the rate of absorption of 1–2 ml hydrothoraces in rabbits most likely overestimated the normal rate by 10-fold (Table 7). Thus the contribution of active liquid absorption relative to that of lymphatic absorption remains to be measured under normal conditions.

C. Clearance by Lymphatic Stomata Versus Mesothelial Absorption

The steady-state pleural liquid protein concentration is relatively low, consistent with microvascular filtration with a high reflection coefficient and absorption via lymphatic stomata that do not restrict the passage of protein. This rather simple explanation for the turnover of pleural liquid contrasts to the more complex one needed if active water and protein reabsorption by the mesothelium were the primary mechanism of absorption. The evidence for transcytosis of protein by mesothelium is inconclusive (see sect. VI*B*). Even if protein were transported by transcytosis, the subsequent route of absorption would be problematic. One route, transcapillary reabsorption of protein, seems improbable in view of a reflection coefficient of 0.7–0.9 measured for pulmonary (190) and systemic capillaries (121). Protein and water reabsorption by the alternative route, interstitial lymphatics, although possible, seems unlikely since hydraulic conductance of interstitium is considerably less than that of lymphatic stomata. Furthermore, if the interstitial lymphatics were the primary route of absorption, it would be difficult to explain how the microvascular filtrate from the parietal pleural capillaries ever reaches the pleural space.

VII. CONCLUDING REMARKS

I have attempted to summarize the pertinent literature within the context of a view of pleural mechanics based on viscous flow concepts as opposed to one based on hydrostatic equilibrium and pleural contact. The concept of fluid lubrication applied to the redistribution of pleural liquid provides a more complete understanding of the forces at work in the pleural space. However, there are two areas in pleural research where our understanding of the basic physiology is incomplete. The first is related to pleural contact. In spite of the lack of direct experimental evidence of pleural contact, the large amount of hyaluronan produced by increased ventilation suggests some role for hyaluronan as a boundary lubricant to reduce shear stress on the mesothelial cell surface and the power loss during breathing. Further work is needed to resolve the relative contributions of boundary and fluid lubrication. The second is related to pleural liquid reabsorption. Although pleural liquid and protein absorption via lymphatic stomata is the straightforward way to explain the available data, the contribution of active transport across the mesothelium to absorption under normal conditions remains to be evaluated.

This research was supported by National Heart, Lung, and Blood Institute Research Grants HL-36597 and HL-40362.

Address for reprint requests and other correspondence: S. J. Lai-Fook, Center for Biomedical Engineering, Wenner-Gren Research Laboratory, Univ. of Kentucky, Lexington, KY 40506-0070 (E-mail: laifook@uky.edu).

REFERENCES

1. **Agostoni E.** Mechanics of the pleural space. *Physiol Rev* 52: 57–128, 1972.
2. **Agostoni E.** Mechanics of the pleural space. In: *Handbook of Physiology. The Respiratory System. Mechanics of Breathing.* Bethesda, MD: Am. Physiol. Soc., 1986, sect. 3, vol. III, pt. 2, chapt. 30, p.531–560.
3. **Agostoni E, Agostoni PG, and Zocchi L.** Pleural liquid pressure in the zone of apposition and in the lung zone. *Respir Physiol* 75: 357–370, 1989.
4. **Agostoni E, Bodega F, and Zocchi L.** Equivalent radius of paracellular "pores" of the mesothelium. *J Appl Physiol* 87: 538–544, 1999.
5. **Agostoni E, Bodega F, and Zocchi L.** Albumin transcytosis from the pleural space. *J Appl Physiol* 93: 1806–1812, 2002.
6. **Agostoni E and D'Angelo E.** The recoil of the most dependent part of the lung. *Respir Physiol* 5: 379–384, 1968.
7. **Agostoni E and D'Angelo E.** Thickness and pressure of the pleural liquid at various heights and with various hydrothoraces. *Respir Physiol* 6: 330–342, 1969.
8. **Agostoni E and D'Angelo E.** Comparative features of the transpulmonary pressure. *Respir Physiol* 11: 76–83, 1970.
9. **Agostoni E and D'Angelo E.** Pleural liquid pressure. *J Appl Physiol* 71: 393–403, 1991.
10. **Agostoni E, D'Angelo E, and Bonanni MV.** Measurements of pleural liquid pressure without cannula. *J Appl Physiol* 26: 258–260, 1969.
11. **Agostoni E, D'Angelo E, and Roncoroni G.** The thickness of the pleural liquid. *Respir Physiol* 5: 1–13, 1968.
12. **Agostoni E and Miserocchi G.** Vertical gradient of transpulmonary pressure with active and artificial lung expansion. *J Appl Physiol* 29: 705–712, 1970.
13. **Agostoni E, Miserocchi G, and Bonnani MV.** Thickness and pressure of the pleural liquid in some mammals. *Respir Physiol* 6: 245–256, 1969.
14. **Agostini E, Taglietti A, and Setnikar I.** Absorption force of the capillaries of the visceral pleura in determination of intrapleural pressure. *Am J Physiol* 191: 277–282, 1957.
15. **Agostoni E and Zocchi L.** Solute-coupled liquid absorption from the pleural space. *Respir Physiol* 81: 19–27, 1990.
16. **Agostoni E and Zocchi L.** Active Na^+ transport and coupled liquid outflow from hydrothoraces of various size. *Respir Physiol* 92: 101–113, 1993.
17. **Agostoni E and Zocchi L.** Mechanisms involved in pleural liquid turnover. *J Appl Physiol* 78: 2329–2330, 1995.
18. **Agostoni E and Zocchi L.** Mechanical coupling and liquid exchanges in the pleural space. *Clin Chest Med* 19: 241–260, 1998.
19. **Agostoni E and Zocchi L.** Starling forces and lymphatic drainage in pleural liquid and protein exchanges. *Respir Physiol* 86: 271–281, 1991.
20. **Agostoni E, Zocchi L, and Agostoni PG.** Pleural liquid pressure at the caudal border of the lung. *Respir Physiol* 75: 117–128, 1989.
21. **Agostoni E, Zocchi L, Agostoni PG, and Macklem PT.** Pleural pressure from abdominal to pulmonary rib cage: sweep of the lung border. *Respir Physiol* 75: 105–115, 1989.

22. **Agostoni E, Zocchi L, and Macklem PT.** Lung border sweep upon phrenic stimulation: dynamic fall in pleural liquid pressure. *Respir Physiol* 77: 379–394, 1989.
23. **Agostoni E, Zocchi L, and Macklem PT.** Transdiaphragmatic pressure and rib motion in the area of apposition during paralysis. *J Appl Physiol* 65: 1296–1300, 1988.
24. **Albert RK and Hubmayr RD.** The prone position eliminates compression of the lungs by the heart. *Am J Respir Crit Care Med* 161: 1660–1665, 2000.
25. **Albert RK, Leasa D, Sanderson M, Robertson HT, and Hlastala MP.** The prone position improves arterial oxygenation and reduces shunt in oleic-acid-induced acute lung injury. *Am Rev Respir Dis* 135: 628–633, 1987.
26. **Albertine KH, Schultz EL, Wiener-Kronish JP, and Staub NC.** Regional differences in pleural lymphatic albumin concentration in sheep. *Am J Physiol Heart Circ Physiol* 252: H64–H70, 1987.
27. **Albertine KH, Wiener-Kronish JP, Bastacky J, and Staub NC.** No evidence of mesothelial cell contact across the costal pleural space in sheep. *J Appl Physiol* 70: 123–134, 1991.
28. **Albertine KH, Wiener-Kronish JP, Roos PJ, and Staub NC.** Structure, blood supply, and lymphatic vessels of the sheep's visceral pleura. *Am J Anat* 165: 277–294, 1982.
29. **Albertine KH, Wiener-Kronish JP, and Staub NC.** The structure of the parietal pleura and its relationship to pleural liquid dynamics in sheep. *Anat Rec* 208: 401–409, 1984.
30. **Allen SJ, Fraser RE, Laurent UB, Reed RK, and Laurent TC.** Turnover of hyaluronan in the rabbit pleural space. *J Appl Physiol* 73: 1457–1460, 1992.
31. **Allen SJ, Gabel J, and Drake R.** Left atrial hypertension causes pleural effusion formation in anesthetized sheep. *Am J Physiol Heart Circ Physiol* 257: H690–H692, 1989.
32. **Amis TC, Jones HA, and Hughes JM.** Effects of posture on inter-regional distribution of pulmonary ventilation in man. *Respir Physiol* 56: 145–167, 1984.
33. **Andrews PM and Porter KR.** The ultrastructural morphology and possible functional significance of mesothelial microvilli. *Anat Rec* 177: 409–426, 1973.
34. **Aukland K and Nicolaysen G.** Interstitial fluid volume: local regulatory mechanisms. *Physiol Rev* 61: 556–643, 1981.
35. **Banchero N, Schwartz PE, Tsakiris AG, and Wood EH.** Pleural and esophageal pressures in the upright body position. *J Appl Physiol* 23: 228–234, 1967.
36. **Bar-Yishay E, Hyatt RE, and Rodarte JR.** Effect of heart weight on distribution of lung surface pressures in vertical dogs. *J Appl Physiol* 61: 712–718, 1986.
37. **Baydur A, Behrakis PK, Zin WA, Jaeger M, and Milic-Emili J.** A simple method for assessing the validity of the esophageal balloon technique. *Am Rev Respir Dis* 126: 788–791, 1982.
38. **Bernaudin JF and Fleury J.** Anatomy of the blood and lymphatic circulation of the pleural serosa. In: *The Pleura in Health and Disease*, edited by Chrétien J, Bignon J, and Hirsch A. New York: Dekker, 1985, p. 101–121.
39. **Bernaudin JF, Jaurand MC, Fleury J, and Bignon J.** Mesothelial cells. In: *The Lung: Scientific Foundations* (1st ed.), edited by Crystal RG, Barnes PJ, West JB, and Weibel ER. Philadelphia, PA: Lippincott-Raven, 1991, vol. 1, p. 631–638.
40. **Bernaudin JF, Theven D, Pinchon MC, Brub-Pascaud M, Bellon B, and Pocidalo JJ.** Protein transfer in hyperoxic induced pleural effusions in the rat. *Exp Lung Res* 10: 23–38, 1986.
41. **Bhattacharya J, Gropper MA, and Staub NC.** Interstitial fluid pressure gradient measured by micropuncture in excised dog lung. *J Appl Physiol* 56: 271–277, 1984.
42. **Bodega F, Zocchi L, and Agostoni E.** Albumin transcytosis in mesothelium. *Am J Physiol Lung Cell Mol Physiol* 282: L3–L11, 2002.
43. **Bodega F, Zocchi L, and Agostoni E.** Macromolecule transfer through mesothelium and connective tissue. *J Appl Physiol* 89: 2165–2173, 2000.
44. **Bodega F, Zocchi L, Cremaschi D, and Agostoni E.** Electrical resistance and ion diffusion through mesothelium. *Respir Physiol* 124: 231–241, 2001.
45. **Bohlen HG, Gore RW, and Hutchins PM.** Comparison of microvascular pressures in normal and spontaneously hypertensive rats. *Microvasc Res* 13: 125–130, 1977.
46. **Bowden FP and Tabor D.** *Friction and Lubrication*. London: Methuen, 1967.
47. **Brandi G.** Frictional forces at the surface of the lung. *Bull Physiopathol Respir* 8: 323–336, 1972.
48. **Broaddus VC and Araya M.** Liquid and protein dynamics using a new minimally invasive pleural catheter in rabbits. *J Appl Physiol* 72: 851–857, 1992.
49. **Broaddus VC, Araya M, Carlton DP, and Bland RD.** Developmental changes in pleural liquid protein concentration in sheep. *Am Rev Respir Dis* 143: 38–41, 1991.
50. **Broaddus VC, Wiener-Kronish JP, Berthiaume Y, and Staub NC.** Removal of pleural liquid and protein by lymphatics in awake sheep. *J Appl Physiol* 64: 384–390, 1988.
51. **Broaddus VC, Wiener-Kronish JP, Laurent TC, and Staub NC.** Clearance of hyaluronan into the pleural space during high pressure pulmonary edema in sheep (Abstract). *FASEB J* 2: 1703, 1988.
52. **Broaddus VC, Wiener-Kronish JP, and Staub NC.** Clearance of lung edema into the pleural space of volume-loaded anesthetized sheep. *J Appl Physiol* 68: 2623–2630, 1990.
53. **Brown RE, Butler JP, Godleski JJ, and Loring SH.** The elephant's respiratory system: adaptations to gravitational stress. *Respir Physiol* 109: 177–194, 1997.
54. **Butler JP, Huang J, Loring SH, Lai-Fook SJ, Wang PM, and Wilson TA.** Model for a pump that drives circulation of pleural fluid. *J Appl Physiol* 78: 23–29, 1995.
55. **Carlsson O, Rosengren BI, and Rippe B.** Transcytosis inhibitor *N*-ethylmaleimide increases microvascular permeability in rat muscle. *Am J Physiol Heart Circ Physiol* 281: H1728–H1733, 2001.
56. **Clough G and Smaje LH.** Simultaneous measurement of pressure in the interstitium and the terminal lymphatics of the cat mesentery. *J Physiol* 283: 457–468, 1978.
57. **Coulam CM and Wood EH.** Regional differences in pleural and esophageal pressures in head-up and head-down positions. *J Appl Physiol* 31: 277–287, 1971.
58. **Courtice FC and Simmonds WT.** Absorption of fluids from the pleural cavities of rabbits and cats. *J Physiol* 109: 117–130, 1949.
59. **Courtice FC and Simmonds WT.** Physiological significance of lymph drainage of the serous cavities and lungs. *Physiol Rev* 34: 419–448, 1954.
60. **Curry FE.** Mechanics and thermodynamics of capillary exchange. In: *Handbook of Physiology. The Cardiovascular System. Microcirculation*. Bethesda, MD: Am. Physiol. Soc., 1984, sect. 2, vol. IV, chapt. 8, p.309–374.
61. **D'Angelo E.** Local alveolar size and transpulmonary pressure in situ and in isolated lungs. *Respir Physiol* 14: 251–266, 1972.
62. **D'Angelo E and Agostoni E.** Continuous recording of pleural surface pressure at various sites. *Respir Physiol* 19: 356–368, 1973.
63. **D'Angelo E, Bonanni MV, Michelini S, and Agostoni E.** Topography of the pleural pressure in rabbits and dogs. *Respir Physiol* 8: 204–229, 1970.
64. **D'Angelo E, Heisler N, and Agostoni E.** Acid-base balance of pleural liquid in dogs. *Respir Physiol* 37: 137–149, 1979.
65. **Deffebach ME, Charan NB, Lakshminarayan S, and Butler J.** The bronchial circulation. *Am Rev Respir Dis* 135: 463–481, 1987.
66. **Douglas WW, Rehder K, Beynen FM, Sessler AD, and Marsh HM.** Improved oxygenation in patients with acute respiratory failure: the prone position. *Am Rev Respir Dis* 115: 559–566, 1977.
67. **Earles NB.** The anatomy of a foetal African elephant, *Elaphus africanus* (*Laxodonta africana*). Part 3, the contents of the thorax, abdomen and skeleton. *Trans R Soc Edin* 56: 203–246, 1929.
68. **Fike CD, Lai-Fook SJ, and Bland RD.** Alveolar liquid pressure in newborn and adult rabbit lungs. *J Appl Physiol* 64: 1629–1635, 1988.
69. **Fingerote R, Fung HY, and Rabkin SW.** Hydraulic permeability of canine and human pericardium in vitro. *Basic Res Cardiol* 75: 764–771, 1980.
70. **Fraser JRE and Laurent TC.** Hyaluronan. In: *Extracellular Matrix*, edited by Comper W. London: Taylor & Francis, 1996, vol. 2, p. 141–197.
71. **Ganesan S and Lai-Fook SJ.** Alveolar liquid pressure measured

in the intact rabbit chest by micropuncture. *J Appl Physiol* 75: 1525–1528, 1993.
72. **Ganesan S, Lai-Fook SJ, and Schurch S.** Alveolar liquid pressures in nonedematous and kerosene-washed rabbit lung by micropuncture. *Respir Physiol* 78: 281–295, 1989.
73. **Ganesan S, Rouch KE, and Lai-Fook SJ.** A finite element analysis of the effect of the abdomen on regional lung expansion. *Respir Physiol* 99: 341–353, 1995.
74. **Glazier JB, Hughes JM, Maloney JE, and West JB.** Vertical gradient of alveolar size in lungs of dogs frozen intact. *J Appl Physiol* 23: 694–705, 1967.
75. **Gray SW and Skandalakis JE.** Development of the pleura. In: *The Pleura in Health and Disease*, edited by Chrétien J, Bignon J, and Hirsch A. New York: Dekker, 1985, p. 3–18.
76. **Grotberg JB and Glucksberg MR.** A buoyancy-driven squeeze-film model of intrapleural fluid dynamics: basic concepts. *J Appl Physiol* 77: 1555–1561, 1994.
77. **Haber R, Grotberg JB, Glucksberg MR, Miserocchi G, Venturoli D, Del Fabbro M, and Waters CM.** Steady-state pleural fluid flow and pressure and the effects of lung buoyancy. *J Biomech Eng* 123: 485–492, 2001.
78. **Hajji MA, Wilson TA, and Lai-Fook SJ.** Improved measurements of the shear modulus and pleural membrane tension of the lung. *J Appl Physiol* 47: 175–181, 1979.
79. **Hatzoglou CH, Gourgoulianis KI, and Molyvdas PA.** Effects of SNP, oubain, and amiloride on electrical potential profile of isolated sheep pleura. *J Appl Physiol* 90: 1565–1569, 2001.
80. **Hills BA.** Graphite-like lubrication of mesothelium by oligolamellar pleural surfactant. *J Appl Physiol* 73: 1034–1039, 1992.
81. **Hills BA, Butler BD, and Barrow RE.** Boundary lubrication imparted by pleural surfactants and their identification. *J Appl Physiol* 53: 463–469, 1982.
82. **Hoffman EA.** Effect of body orientation on regional lung expansion: a computed tomographic approach. *J Appl Physiol* 59: 468–480, 1985.
83. **Hoffman EA, Lai-Fook SJ, Wei J, and Wood EH.** Regional pleural surface expansile forces in intact dogs by wick catheters. *J Appl Physiol* 55: 1523–1529, 1983.
84. **Hoffman EA and Ritman EL.** Effect of body orientation on regional lung expansion in dog and sloth. *J Appl Physiol* 59: 481–491, 1985.
85. **Hogg JC and Nepszy S.** Regional lung volume and pleural pressure gradient estimated from lung density in dogs. *J Appl Physiol* 27: 198–203, 1969.
86. **Hogg JC, Stein L, Martin R, and Macklem PT.** The interaction of the lung and chest wall in dogs. *Respir Physiol* 27: 207–221, 1976.
87. **Hoppin FG Jr, Green ID, and Mead J.** Distribution of pleural surface pressure in dogs. *J Appl Physiol* 27: 863–873, 1969.
88. **Hubmayr RD, Walters BJ, Chevalier PA, Rodarte JR, and Olson LE.** Topographic distribution of regional lung volume in anesthetized dogs. *J Appl Physiol* 54: 1048–1056, 1983.
89. **Hyatt RE, Bar-Yishay E, and Abel MD.** Influence of the heart on the vertical gradient of transpulmonary pressure in dogs. *J Appl Physiol* 58: 52–57, 1985.
90. **Kaneko K, Milic-Emili J, Dolovich MB, Dawson A, and Bates DV.** Regional distribution of ventilation and perfusion as a function of body position. *J Appl Physiol* 21: 767–777, 1966.
91. **Kaplowitz MR and Lai-Fook SJ.** Pressure and dimensions of pleural liquid at lobar margins of dogs and rabbits (Abstract). *Federation Proc* 44: 1027, 1985.
92. **Kim KJ, Critz AM, and Crandall ED.** Transport of water and solutes across sheep visceral pleura. *Am Rev Respir Dis* 120: 883–892, 1979.
93. **Kinasewitz GT and Fishman AP.** Influence of alterations in Starling forces on visceral pleural fluid movement. *J Appl Physiol* 51: 671–677, 1981.
94. **Kinasewitz GT, Groome LJ, Marshall RP, and Diana JN.** Permeability of the canine visceral pleura. *J Appl Physiol* 55: 121–130, 1983.
95. **Kinasewitz GT, Groome LJ, Marshall RP, and Diana JN.** Role of pulmonary lymphatics and interstitium in visceral pleural fluid exchange. *J Appl Physiol* 56: 355–363, 1984.
96. **Krueger JJ, Bain T, and Patterson JL.** Elevation gradient of intrathoracic pressure. *J Appl Physiol* 16: 465–468, 1961.
96a. **Lai J, Gouldstone A, Butler JP, Federspiel WJ, and Loring SH.** Relative motion of the lung and chest wall promotes uniform pleural space thickness. *Respir Physiol Neurobiol* 131: 233–243, 2002.
97. **Lai-Fook SJ.** Mechanics of the pleural space: fundamental concepts. *Lung* 165: 249–267, 1987.
98. **Lai-Fook SJ, Beck KC, and Southorn PA.** Pleural liquid pressure measured by micropipettes in rabbits. *J Appl Physiol* 56: 1633–1639, 1984.
99. **Lai-Fook SJ, Brown LV, Maudgalya VS, Knapp CF, and Ganesan S.** Effect of increased acceleration on regional pleural pressure in dogs. *J Appl Physiol* 71: 611–619, 1991.
100. **Lai-Fook SJ and Kaplowitz MR.** Pleural protein concentration and liquid volume in spontaneously hypertensive rats. *Microvasc Res* 35: 101–108, 1988.
101. **Lai-Fook SJ and Kaplowitz MR.** Pleural space thickness in situ by light microscopy in five mammalian species. *J Appl Physiol* 59: 603–610, 1985.
102. **Lai-Fook SJ, Price DC, and Staub NC.** Liquid thickness vs. vertical pressure gradient in a model of the pleural space. *J Appl Physiol* 62: 1747–1754, 1987.
103. **Lai-Fook SJ and Rodarte JR.** Pleural pressure distribution and its relationship to lung volume and interstitial pressure. *J Appl Physiol* 70: 967–978, 1991.
104. **Lai-Fook SJ and Wang PM.** Dynamics of pleural liquid: mechanical factors affecting its formation and regional distribution. In: *Lung Biology in Health and Disease. Complexities in Structure and Function of the Lung*, edited by Hlastala MP and Robertson HT. New York: Dekker, 1998, p. 123–149.
106. **Landis EM and Pappenheimer JR.** Exchange of substances through the capillary wall. In: *Handbook of Physiology. Circulation*. Washington, DC: Am. Physiol. Soc., 1963, sect. 2, vol. II, p. 961–1034.
107. **Laurent TC and Fraser JRE.** Hyaluronan (Abstract). *FASEB J* 6: 2397–2404, 1992.
108. **Leak LV and Rahil K.** Permeability of the diaphragm mesothelium: the ultrastructural basis for "stomata." *Am J Anat* 151: 557–593, 1978.
109. **Lebel L, Smith L, Risberg B, Gerdin B, and Laurent TC.** Effect of increased hydrostatic pressure on lymphatic elimination of hyaluronan from sheep lung. *J Appl Physiol* 64: 1327–1332, 1988.
110. **Leckie WJ and Tothill P.** Albumin turnover in pleural effusions. *Clin Sci* 29: 339–352, 1965.
111. **Lillington GA, Fowler WS, Miller RD, and Helmholtz HF Jr.** Nitrogen clearance rates of right and left lungs in different positions. *J Clin Invest* 38: 2026–2034, 1959.
112. **Liu S, Margulies SS, and Wilson TA.** Deformation of the dog lung in the chest wall. *J Appl Physiol* 68: 1979–1987, 1990.
113. **Loring SH, Yoshino K, Kimball WR, and Barnas GM.** Gravitational and shear-induced pressure gradients in the abdomen. *J Appl Physiol* 77: 1375–1382, 1994.
114. **Macklem PT, Zocchi L, and Agostoni E.** Pleural pressure between diaphragm and rib cage during inspiratory muscle activity. *J Appl Physiol* 65: 1286–1295, 1988.
115. **Mariassy AT and Wheeldon EB.** The pleura: a combined light microscopic, scanning and transmission electron microscopic study in the sheep. I. Normal pleura. *Exp Lung Res* 4: 293–314, 1983.
116. **McLaughlin RF, Tyler WS, and Canada RO.** A study of the subgross pulmonary anatomy of various mammals. *Am J Anat* 108: 149–159, 1961.
117. **McMahon SM, Proctor DF, and Permutt S.** A model to evaluate pleural surface pressure measuring devices. *J Appl Physiol* 27: 886–891, 1969.
118. **McMahon SM, Proctor DF, and Permutt S.** Pleural surface pressure in dogs. *J Appl Physiol* 27: 881–885, 1969.
119. **Mead J.** Functional significance of the area of apposition of diaphragm to rib cage. *Am Rev Respir Dis Suppl* 119: 31–32, 1979.
120. **Mellins RB, Levine OR, and Fishman AP.** Effect of systemic and pulmonary venous hypertension on pleural and pericardial fluid accumulation. *J Appl Physiol* 29: 564–569, 1970.

121. **Michel CC.** Fluid movement through capillary walls. In: *Handbook of Physiology. The Cardiovascular System. Microcirculation.* Bethesda, MD: Am. Physiol. Soc., 1984, sect. 2, vol. IV, chapt. 9, p. 375–410.
122. **Milic-Emili J.** Static distribution of lung volume. In: *Handbook of Physiology. The Respiratory System. Mechanics of Breathing.* Bethesda, MD: Am. Physiol. Soc., 1986, sect. 3, vol. III, pt. 2, chapt. 31, p. 561–574.
123. **Milic-Emili J, Henderson JA, Dolovich MB, Trop D, and Kaneko K.** Regional distribution of inspired gas in the lung. *J Appl Physiol* 21: 749–759, 1966.
124. **Miniati M, Parker JC, Pistolesi M, Cartledge JT, Martin DJ, Giuntini C, and Taylor AE.** Reabsorption kinetics of albumin from the pleural space of dogs. *Am J Physiol Heart Circ Physiol* 255: H375–H385, 1988.
125. **Miserocchi G.** Pleural pressure and fluid transport. In: *The Lung: Scientific Foundations*, edited by Crystal RG and West JB. New York: Raven, 1991, p. 885–893.
126. **Miserocchi G.** Physiology and pathophysiology of pleural fluid turnover. *Eur Respir J* 10: 219–225, 1997.
127. **Miserocchi G and Agostoni E.** Contents of the pleural space. *J Appl Physiol* 30: 208–213, 1971.
128. **Miserocchi G and Agostoni E.** Pleural liquid and surface pressures at various lung volume. *Respir Physiol* 39: 315–326, 1980.
129. **Miserocchi G, Kelly S, and Negrini D.** Pleural and extrapleural interstitial liquid pressure measured by cannulas and micropipettes. *J Appl Physiol* 65: 555–562, 1988.
130. **Miserocchi G, Mariani E, and Negrini D.** Role of the diaphragm in setting liquid pressure in serous cavities. *Respir Physiol* 50: 381–392, 1982.
131. **Miserocchi G, Nakamura T, Mariani E, and Negrini D.** Pleural liquid pressure over the interlobar mediastinal and diaphragmatic surfaces of the lung. *Respir Physiol* 46: 61–69, 1981.
132. **Miserocchi G and Negrini D.** Contribution of Starling and lymphatic flows to pleural liquid exchanges in anesthetized rabbits. *J Appl Physiol* 61: 325–330, 1986.
133. **Miserocchi G and Negrini D.** Pleural space: pressures and fluid dynamics. In: *The Lung: Scientific Foundations* (2nd ed.), edited by Crystal RG, Barnes PJ, West JB, and Weibel ER. Philadelphia, PA: Lippincott-Raven, 1997, vol. 1, p. 1217–1726.
134. **Miserocchi G, Negrini D, and Gonano C.** Direct measurement of interstitial pulmonary pressure in in situ lung with intact pleural space. *J Appl Physiol* 69: 2168–2174, 1990.
135. **Miserocchi G, Negrini D, and Gonano C.** Parenchymal stress affects interstitial and pleural pressures in in-situ lung. *J Appl Physiol* 71: 1967–1972, 1991.
136. **Miserocchi G, Negrini D, Mariani E, and Passafaro M.** Reabsorption of saline- or plasma-induced hydrothorax. *J Appl Physiol* 54: 1574–1578, 1983.
137. **Miserocchi G, Negrini D, and Mortola J.** Comparative features of Starling-lymphatic interaction at the pleural level in mammals. *J Appl Physiol* 56: 1151–1156, 1984.
138. **Miserocchi G, Negrini D, Mukenge S, Turconi P, and DelFabbro M.** Liquid drainage through the peritoneal diaphragmatic surface. *J Appl Physiol* 66: 1579–1585, 1989.
139. **Miserocchi G, Negrini D, Pistolesi M, Bellina CR, Gilardi MC, Bettinardi V, and Rossitto F.** Intrapleural liquid flow down a gravity-dependent hydraulic pressure gradient. *J Appl Physiol* 64: 577–584, 1988.
140. **Miserocchi G, Pistolesi M, Miniati M, Bellina CR, Negrini D, and Giuntini C.** Pleural liquid pressure gradients and intrapleural distribution of injected bolus. *J Appl Physiol* 56: 526–532, 1984.
141. **Miserocchi G, Venturoli D, Negrini D, and Del-Fabbro M.** Model of pleural fluid turnover. *J Appl Physiol* 75: 1798–1806, 1993.
142. **Miserocchi G, Venturoli D, Negrini D, Gilardi MC, and Bellina R.** Intrapleural fluid movements described by a porous flow model. *J Appl Physiol* 73: 2511–2516, 1992.
143. **Moe SM and Lai-Fook SJ.** Effect of concentration on albumin restriction and diffusion in the excised rat diaphragm. *Microvasc Res* 65: 96–108, 2003.
144. **Moe SM and Lai-Fook SJ.** Transcytosis inhibitor nocodazole increases diffusive permeability across rabbit pericardium (Abstract). *FASEB J* 17: A86, 2003.
145. **Moe SM and Lai-Fook SJ.** Transcytosis inhibitor nocodazole increases hydraulic conductivity of rabbit pericardium (Abstract). *FASEB J* 17: A86, 2003.
146. **Negrini D, Ballard ST, and Benoit JN.** Contribution of lymphatic myogenic activity and respiratory movements to pleural liquid flow. *J Appl Physiol* 76: 2267–2274, 1994.
147. **Negrini D, Capelli C, Morini M, and Miserocchi G.** Gravity-dependent distribution of parietal subpleural interstitial pressure. *J Appl Physiol* 63: 1912–1918, 1987.
148. **Negrini D, Del Fabbro M, and Venturoli D.** Fluid exchanges across the parietal peritoneal and pleural mesothelia. *J Appl Physiol* 74: 1779–1784, 1993.
149. **Negrini D and Fabbro MD.** Subatmospheric pressure in the rabbit pleural lymphatic networks. *J Physiol* 520: 761–769, 1999.
150. **Negrini D and Miserocchi G.** Size-related differences in parietal extrapleural and pleural liquid pressure distribution. *J Appl Physiol* 67: 1967–1972, 1989.
151. **Negrini D, Mukenge S, Del Fabbro M, Gonano C, and Miserocchi G.** Distribution of diaphragmatic lymphatic stomata. *J Appl Physiol* 70: 1544–1549, 1991.
152. **Negrini D, Pistolesi M, Miniati M, Bellina R, Giuntini C, and Miserocchi G.** Regional protein absorption rates from the pleural cavity in dogs. *J Appl Physiol* 58: 2062–2067, 1985.
153. **Negrini D, Reed RK, and Miserocchi G.** Permeability-surface area product and reflection coefficient of the parietal pleura in dogs. *J Appl Physiol* 71: 2543–2547, 1991.
154. **Negrini D, Townsley MI, and Taylor AE.** Hydraulic conductivity of canine parietal pleura in vivo. *J Appl Physiol* 69: 438–442, 1990.
155. **Negrini D, Venturoli D, Townsley MI, and Reed RK.** Permeability of parietal pleura to liquid and proteins. *J Appl Physiol* 76: 627–633, 1994.
156. **Ogston AG and Stanier JE.** The physiological function of hyaluronic acid in synovial fluid: viscous, elastic and lubricant properties. *J Physiol* 119: 244–252, 1953.
157. **Oldmixon EH and Hoppin FG Jr.** Comparison of amounts of collagen and elastin in pleura and parenchyma of dog lung. Morphometric quantification of connective tissue in pleura and alveolar parenchyma. *J Appl Physiol* 56: 1383–1388, 1984.
158. **Olson LE and Hoffman EA.** Lung volume and distribution of regional air content determined by cine X-ray CT of pneumonectomized rabbits. *J Appl Physiol* 76: 1774–1785, 1994.
159. **Olson LE and Lai-Fook SJ.** Pleural liquid pressure measured with rib capsules in anesthetized ponies. *J Appl Physiol* 64: 102–107, 1988.
160. **Olson LE and Wardle RL.** Pleural pressure as a function of body position in rabbits. *J Appl Physiol* 69: 336–344, 1990.
161. **Parameswaran S, Brown LV, Ibbott GS, and Lai-Fook SJ.** Effect of concentration and hyaluronidase on albumin diffusion across rabbit mesentery. *Microcirculation* 6: 117–126, 1999.
162. **Parameswaran S, Brown LV, Ibbott GS, and Lai-Fook SJ.** Hydraulic conductivity, albumin reflection and diffusion coefficients of pig mediastinal pleura. *Microvasc Res* 58: 114–127, 1999.
163. **Parameswaran S, Brown LV, and Lai-Fook SJ.** Effect of flow on hydraulic conductivity and reflection coefficient of rabbit mesentery. *Microcirculation* 5: 265–274, 1998.
164. **Payne DK, Kinasewitz GT, and Gonzalez E.** Comparative permeability of canine visceral and parietal pleura. *J Appl Physiol* 65: 2558–2564, 1988.
165. **Pegram BL and Bishop VS.** An evaluation of the pericardial sac as a safety factor during tamponade. *Cardiovasc Res* 9: 715–721, 1975.
166. **Perez F, Fernandez P, Hernaiz MI, Jackson EG, Lai-Fook SJ, and Boynton BR.** Pleural pressure measured in the zone of apposition of diaphragm to rib cage in rabbits. *Lung* 171: 345–353, 1993.
167. **Policard A and Galy P.** *La Plèvre.* Paris*:* Masson, 1942.
168. **Proctor DF, Caldini P, and Permutt S.** The pressure surrounding the lungs. *Respir Physiol* 5: 130–144, 1968.
169. **Rehder K, Hatch DJ, Sessler AD, and Fowler WS.** The function of each lung of anesthetized and paralyzed man during mechanical ventilation. *Anesthesiology* 37: 16–26, 1972.
170. **Rehder K and Marsh HM.** Respiratory mechanics during anesthesia and mechanical ventilation. In: *Handbook of Physiology. The Respiratory System. Mechanics of Breathing.* Bethesda, MD: Am. Physiol. Soc., 1986, sect. 3, vol. III, pt. 2, chapt. 43, p. 737–754.

171. **Rehder K, Sessler AD, and Rodarte JR.** Regional intrapulmonary gas distribution in awake and anesthetized-paralyzed man. *J Appl Physiol* 42: 391–402, 1977.
172. **Rippe B and Taylor A.** NEM and filipin increase albumin transport in lung microvessels. *Am J Physiol Heart Circ Physiol* 280: H34–H41, 2001.
173. **Rosselli RJ and Harris TR.** Lung fluid and macromolecular transport. In: *Respiratory Physiology: An Analytical Approach*, edited by Chang HK and Paiva M. New York: Dekker, 1989, p. 644.
174. **Roussos CS, Fukuchi Y, Macklem PT, and Engel LA.** Influence of diaphragmatic contraction on ventilation distribution in horizontal man. *J Appl Physiol* 40: 417–424, 1976.
175. **Rutishauser WJ, Banchero N, Tsakiris AG, Edmundowicz AC, and Wood EH.** Pleural pressures at dorsal and ventral sites in supine and prone body positions. *J Appl Physiol* 21: 1500–1510, 1966.
176. **Rutishauser WJ, Banchero N, Tsakiris AG, and Wood EH.** Effect of gravitational and inertial forces on pleural and esophageal pressures. *J Appl Physiol* 22: 1041–1052, 1967.
177. **Sahn SA, Wilcox ML, Good JT Jr, Potts DE, and Filley GF.** Characteristics of normal rabbit pleural fluid. Physiologic and biochemical implications. *Lung* 156: 63–69, 1979.
178. **Sarkos S, Hatzoglou CH, Dahabre J, Gourgoulianis KI, and Molyvdas PA.** Effect of amiloride in human and sheep parietal pleura. *Respir Physiol Neurobiol* 132: 233–237, 2002.
179. **Schmid-Schonbein GW.** Microlymphatics and lymph flow. *Physiol Rev* 70: 987–1028, 1990.
180. **Setnikar I, Taglietti A, and Agostoni E.** La cinetica del liquido pleurico studiata per mezza di albumina marcata con ^{131}I. *Boll Soc Ital Biol Sper* 33: 1650–1652, 1957.
181. **Shinohara H.** Distribution of lymphatic stomata on the pleural surface of the thoracic cavity and the surface topography of the pleural mesothelium in the golden hamster. *Anat Rec* 249: 16–23, 1997.
182. **Speels KR.** Comparative studies in lung mechanics based on a survey of literature data. *Respir Physiol* 8: 37–57, 1969.
183. **Stahl WR.** Scaling of respiratory variables in mammals. *J Appl Physiol* 22: 453–460, 1967.
184. **Starling EH.** On the absorption of fluids from the connective tissue spaces. *J Physiol* 19: 312–326, 1896.
185. **Staub NC.** Pulmonary edema. *Physiol Rev* 54: 678–811, 1974.
186. **Staub NC, Wiener-Kronish JP, and Albertine KH.** Transport through the pleura. In: *The Pleura in Health and Disease*, edited by Chrétien J, Bignon J, and Hirsch A. New York: Dekker, 1985, p. 188.
187. **Stewart PB.** The rate of formation and lymphatic removal of fluid in pleural effusions. *J Clin Invest* 42: 258–262, 1963.
188. **Stewart PB and Burgen ASV.** The turnover of fluid in the dog's pleural cavity. *J Lab Clin Med* 52: 212–230, 1958.
189. **Surprenant EL and Rodbard S.** A hydrostatic pressure gradient in the pleural sac. *Am Heart J* 66: 215–220, 1963.
190. **Taylor AE and Parker JC.** Pulmonary interstitial space and lymphatics. In: *Handbook of Physiology. The Respiratory System. Circulation and Nonrespiratory Functions*. Bethesda, MD: Am. Physiol. Soc., 1985, sect. 3, vol. I, chapt. 4, p. 167–230.
191. **Thurlbeck WM and Marshall RM.** Topography of esophageal pressure in the dog. *J Appl Physiol* 34: 590–596, 1973.
192. **Townsley MI, Negrini D, and Ardell JL.** Regional blood flow to canine parietal pleura and internal intercostal muscle. *J Appl Physiol* 70: 97–102, 1991.
193. **Turner JM, Mead J, and Wohl ME.** Elasticity of human lungs in relation to age. *J Appl Physiol* 25: 664–671, 1968.
194. **Urmey WF, DeTroyer A, Kelly KB, and Loring SH.** Pleural pressure increases during inspiration in the zone of apposition of diaphragm to rib cage. *J Appl Physiol* 65: 2207–2212, 1988.
195. **Villarruel S, Ibbott GS, and Lai-Fook SJ.** Effect of concentration and hydration on restriction of albumin by lung interstitium. *Microvasc Res* 63: 27–40, 2002.
196. **Wang NS.** The regional difference of pleural mesothelial cells in rabbits. *Am Rev Respir Dis* 110: 623–633, 1974.
197. **Wang NS.** The preformed stomas connecting the pleural cavity and the lymphatics in the parietal pleura. *Am Rev Respir Dis* 111: 12–20, 1975.
198. **Wang NS.** Anatomy and physiology of the pleural space. *Clin Chest Med* 6: 3–16, 1985.
199. **Wang NS.** Mesothelial cells in situ. In: *The Pleura in Health and Disease*, edited by Chrétien J, Bignon J, and Hirsch A. New York: Dekker, 1985, p. 23–42.
200. **Wang NS.** Anatomy of the pleura. *Clin Chest Med* 19: 229–240, 1998.
201. **Wang PM and Lai-Fook SJ.** Upward flow of pleural liquid near lobar margins due to cardiogenic motion. *J Appl Physiol* 73: 2314–2319, 1992.
202. **Wang PM and Lai-Fook SJ.** Effect of ventilation frequency and tidal volume on pleural space thickness in rabbits. *J Appl Physiol* 75: 1836–1841, 1993.
203. **Wang PM and Lai-Fook SJ.** Effect of ventilation frequency on fluid filtration into the pleural space of rabbits (Abstract). *FASEB J* 8: A690, 1994.
204. **Wang PM and Lai-Fook SJ.** Effect of mechanical ventilation on regional variation of pleural liquid thickness in rabbits. *Lung* 175: 165–173, 1997.
205. **Wang PM and Lai-Fook SJ.** Effects of ventilation on hyaluronan and protein concentration in pleural liquid of anesthetized and conscious rabbits. *Lung* 176: 309–324, 1998.
206. **Wang PM and Lai-Fook SJ.** Regional pleural filtration and absorption measured by fluorescent tracers in rabbits. *Lung* 177: 289–309, 1999.
207. **Wang PM and Lai-Fook SJ.** Pleural tissue hyaluronan produced by postmortem ventilation in rabbits. *Lung* 178: 1–12, 2000.
208. **Waters CM, Glucksberg MR, Depaola N, Chang J, and Grotberg JB.** Shear stress alters pleural mesothelial cell permeability in culture. *J Appl Physiol* 81: 448–458, 1996.
209. **West JB.** Snorkel breathing in the elephant explains the unique anatomy of its pleura. *Respir Physiol* 126: 1–8, 2001.
210. **West JB and Matthews FL.** Stresses, strains, and surface pressures in the lung caused by its weight. *J Appl Physiol* 32: 332–345, 1972.
211. **Wiener CM, Kirk W, and Albert RK.** Prone position reverses the gravitational distribution of perfusion in dog lungs with oleic acid-induced injury. *J Appl Physiol* 68: 1386–1392, 1990.
212. **Wiener-Kronish JP, Albertine KH, Licko V, and Staub NC.** Protein egress and entry rates in pleural fluid and plasma in sheep. *J Appl Physiol* 56: 459–463, 1984.
213. **Wiener-Kronish JP and Broaddus VC.** Interrelationship of pleural and pulmonary interstitial liquid. *Annu Rev Physiol* 55: 209–226, 1993.
214. **Wiener-Kronish JP, Gropper MA, and Lai-Fook SJ.** Pleural liquid pressure in dogs measured using a rib capsule. *J Appl Physiol* 59: 597–602, 1985.
215. **Yang QY, Kaplowitz MR, and Lai-Fook SJ.** Regional variations in lung expansion in rabbits: prone vs. supine positions. *J Appl Physiol* 67: 1371–1376, 1989.
216. **Yang QH and Lai-Fook SJ.** Effect of lung inflation on regional lung expansion in supine and prone rabbits. *J Appl Physiol* 71: 76–82, 1991.
217. **Zawieja DC, Garcia C, and Granger HJ.** Oxygen radicals, enzymes, and fluid transport through pericardial interstitium. *Am J Physiol Heart Circ Physiol* 262: H136–H143, 1992.
218. **Zocchi L and Agostoni E.** Effect of beta-adrenergic blockade or stimulation on net rate of hydrothorax absorption. *Respir Physiol* 97: 347–356, 1994.
219. **Zocchi L, Agostoni E, and Cremaschi D.** Electrolyte transport across the pleura of rabbits. *Respir Physiol* 86: 125–138, 1991.
220. **Zocchi L, Agostoni E, and Cremaschi D.** Beta-agonist activation of an amiloride-insensitive transport mechanism in rabbit pleura. *Respir Physiol* 100: 7–13, 1995.
221. **Zocchi L, Agostoni E, and Raffaini A.** Effect of phloridzin on net rate of liquid absorption from the pleural space of rabbits. *Exp Physiol* 81: 957–967, 1996.
222. **Zocchi L, Cremaschi D, and Agostoni E.** Liquid volume and Na^+ and mannitol concentration in hypertonic mannitol-Ringer hydrothorax. *Respir Physiol* 89: 341–351, 1992.
223. **Zocchi L, Raffaini A, and Agostoni E.** Effect of adrenaline and alpha-agonists on net rate of liquid absorption from the pleural space of rabbits. *Exp Physiol* 82: 507–520, 1997.
224. **Zocchi L, Raffaini A, Agostoni E, and Cremaschi D.** Diffusional permeability of rabbit mesothelium. *J Appl Physiol* 85: 471–477, 1998.